J Physiol 593.6 (2015) pp 1459–1477

The Journal of Physiology

Inositol-1,4,5-trisphosphate induced Ca^{2+} release and excitation–contraction coupling in atrial myocytes from normal and failing hearts

Felix Hohendanner[1], Stefanie Walther[1], Joshua T. Maxwell[1], Sarah Kettlewell[2], Sawsan Awad[3], Godfrey L. Smith[2], Vassyl A. Lonchyna[4] and Lothar A. Blatter[1]

[1] *Department of Molecular Biophysics and Physiology, Rush University Medical Center, Chicago, IL 60612, USA*
[2] *Institute of Cardiovascular and Medical Sciences, University of Glasgow, Glasgow G12 8QQ, UK*
[3] *Rush Center for Congenital Heart Disease, Rush University Medical Center, Chicago, IL 60612, USA*
[4] *Section of Cardiac and Thoracic Surgery, The University of Chicago Medicine, Chicago, IL, USA*

Key points

- Impaired calcium (Ca^{2+}) signalling is the main contributor to depressed ventricular contractile function and occurrence of arrhythmia in heart failure (HF).
- Here we report that in atrial cells of a rabbit HF model, Ca^{2+} signalling is enhanced and we identified the underlying cellular mechanisms. Enhanced Ca^{2+} transients (CaTs) are due to upregulation of inositol-1,4,5-trisphosphate receptor induced Ca^{2+} release (IICR) and decreased mitochondrial Ca^{2+} sequestration.
- Enhanced IICR, however, together with an increased activity of the sodium–calcium exchange mechanism, also facilitates spontaneous Ca^{2+} release in form of arrhythmogenic Ca^{2+} waves and spontaneous action potentials, thus enhancing the arrhythmogenic potential of atrial cells.
- Our data show that enhanced Ca^{2+} signalling in HF provides atrial cells with a mechanism to improve ventricular filling and to maintain cardiac output, but also increases the susceptibility to develop atrial arrhythmias facilitated by spontaneous Ca^{2+} release.

Abstract We studied excitation–contraction coupling (ECC) and inositol-1,4,5-triphosphate (IP_3)-dependent Ca^{2+} release in normal and heart failure (HF) rabbit atrial cells. Left ventricular HF was induced by combined volume and pressure overload. In HF atrial myocytes diastolic $[Ca^{2+}]_i$ was increased, action potential (AP)-induced Ca^{2+} transients (CaTs) were larger in amplitude, primarily due to enhanced Ca^{2+} release from central non-junctional sarcoplasmic reticulum (SR) and centripetal propagation of activation was accelerated, whereas HF ventricular CaTs were depressed. The larger CaTs were due to enhanced IP_3 receptor-induced Ca^{2+} release (IICR) and reduced mitochondrial Ca^{2+} buffering, consistent with a reduced mitochondrial density and Ca^{2+} uptake capacity in HF. Elementary IP_3 receptor-mediated Ca^{2+} release events (Ca^{2+} puffs) were more frequent in HF atrial myoctes and were detected more often in central regions of the non-junctional SR compared to normal cells. HF cells had an overall higher frequency of spontaneous Ca^{2+} waves and a larger fraction of waves (termed arrhythmogenic Ca^{2+} waves) triggered APs and global CaTs. The higher propensity of arrhythmogenic Ca^{2+} waves resulted from the combined action of enhanced IICR and increased activity of sarcolemmal Na^{+}–Ca^{2+} exchange depolarizing the cell membrane. In conclusion, the data support the hypothesis that in atrial myocytes from hearts with left ventricular failure, enhanced CaTs during ECC exert positive inotropic effects on atrial contractility which facilitates ventricular filling and contributes to maintaining cardiac output. However, HF atrial cells were also more susceptible to developing arrhythmogenic Ca^{2+} waves which might form the substrate for atrial rhythm disorders frequently encountered in HF.

DOI: 10.1113/jphysiol.2014.283226

(Received 27 August 2014; accepted after revision 10 November 2014; first published online 18 November 2014)
Corresponding author L. A. Blatter: Department of Molecular Biophysics and Physiology, Rush University Medical Center, 1750 W. Harrison Street, Chicago, IL 60612, USA. Email: lothar_blatter@rush.edu

Abbreviations AF, atrial fibrillation; Ang II, angiotensin II; AP, action potential; 2-APB, 2-aminoethoxydiphenyl borate; BSA, bovine serum albumin; $[Ca^{2+}]_i$, cytosolic free Ca^{2+} concentration; $[Ca^{2+}]_{mito}$, mitochondrial free Ca^{2+} concentration; $[Ca^{2+}]_{SR}$, sarcoplasmic reticulum free Ca^{2+} concentration; CaT, Ca^{2+} transient; CICR, Ca^{2+}-induced Ca^{2+}release; CRU, Ca^{2+} release unit; ECC, excitation–contraction coupling; FDHM, full duration at half-maximum; FIRE, fluorescent IP_3-responsive element; FRET, florescence resonance energy transfer; FWHM, full width at half-maximum; GFP, green fluorescent protein; GPCR, G_q-protein coupled receptor; HF, heart failure; IICR, IP_3-induced Ca^{2+}release; IP_3, inositol-1,4,5-trisphosphate; IP_3R, IP_3 receptor; j-SR, junctional sarcoplasmic reticulum; LTCC, L-type Ca^{2+} channel; MCU, mitochondrial calcium uniporter; NCX, Na^+–Ca^{2+} exchange; nj-SR, non-junctional sarcoplasmic reticulum; RyR, ryanodine receptor; SEA, SEA-0400, 2-[4-[(2,5-diuorophenyl) methoxy]phenoxy]-5-ethoxyaniline; SERCA, sarcoplasmic–endoplasmic reticulum Ca^{2+} ATPase; SR, sarcoplasmic reticulum; TTP, time to peak

Introduction

Excitation–contraction coupling (ECC) refers to the process that links action potential-dependent membrane depolarization, elevation of cytosolic Ca^{2+} levels ($[Ca^{2+}]_i$) and force development in cardiac myocytes. Disturbances of ECC play a crucial role in cardiac disease resulting in contractile dysfunction and arrhythmogenesis. Atrial contraction is an important determinant of ventricular filling ('atrial kick') and it can contribute up to 40% of the end-diastolic ventricular filling during periods of increased haemodynamic demands, e.g. during exercise (Rahimtoola *et al.* 1975; Nicod *et al.* 1986). In patients with systolic heart failure (HF), the atrial contribution to the diastolic filling of an impaired ventricle becomes increasingly important to maintain cardiac output (Bonow *et al.* 1983; Raymond *et al.* 1998). Furthermore, such patients are especially prone to develop rhythm disorders like atrial fibrillation, the most common form of cardiac arrhythmia, which not only increase the risk of stroke, but also eliminate the atrial kick. The consequence of diminished atrial contractility is a reduced overall blood pumping capacity of the heart by up to a third, which in turn worsens symptoms of HF and facilitates its progression (Alpert *et al.* 1988). At the single cell level atrial Ca^{2+} signalling during ECC shows properties distinctly different from ventricular cells. These differences can largely be attributed to structural and functional differences in the organization of the couplon (Bootman *et al.* 2006) and the Ca^{2+} release units (CRUs) (Chen-Izu *et al.* 2006; Li *et al.* 2012). The couplon is the basic unit of ECC and refers to the ultrastructural arrangement of the sarcoplasmic reticulum (SR) membrane hosting ryanodine receptor (RyR) Ca^{2+} release channels and the sarcolemmal membrane containing L-type Ca^{2+} channels (LTCCs), only separated by a narrow gap of a few nanometres. The fact that the LTCCs directly face clusters of RyRs in CRUs assures activation of RyRs despite their rather low cytosolic Ca^{2+} sensitivity (Cannell & Kong, 2012). These SR regions are referred to as junctional SR (j-SR) where Ca^{2+} entry through LTCCs allows for an efficient activation of a cluster of RyRs forming a CRU by a process termed Ca^{2+} induced Ca^{2+} release (CICR; Cannell *et al.* 1987; Sheehan & Blatter, 2003). In ventricular cells, invaginations of the sarcolemmal membrane organized in a sarcomeric pattern and known as t-tubules create couplons throughout the entire volume of the cell and allow for rapid synchronous release of Ca^{2+} from CRUs. Atrial cells of many species, however, are either devoid of or show very sparse t-tubules, resulting in a rather inhomogenous distribution of the structures involved in Ca^{2+} handling and consequently the spatio-temporal organization of the cytosolic Ca^{2+} signal during ECC. In the subsarcolemmal space, the sarcolemmal membrane is located in close vicinity to the SR (j-SR). Here LTCCs directly face CRUs, resembling the ultrastructural arrangement found in couplons of ventricular cells (Stern *et al.* 1999) and are referred to as peripheral couplings (Kockskamper *et al.* 2001). However in more central regions of the cytosol where t-tubules are absent, abundant RyRs of the non-junctional SR (nj-SR) are found where CRUs are not associated with LTCCs and activation of RyRs relies on centripetal Ca^{2+} diffusion and propagation (Coombes & Timofeeva, 2003; Thul *et al.* 2012; Trafford *et al.* 2013). As a consequence, during ECC striking differences in the shape, magnitude and kinetics of subcellular Ca^{2+} transients (CaTs) are observed: upon action potential-dependent membrane depolarization fast and high-amplitude CaTs in the subsarcolemmal space are observed first that result from CICR from j-SR elicited by Ca^{2+} currents through LTCCs. Centripetal Ca^{2+} diffusion activates CICR from nj-SR CRUs resulting in propagation of CICR towards the cell centre in a Ca^{2+} wave-like fashion (Huser *et al.* 1996; Kockskamper *et al.* 2001; Sheehan & Blatter, 2003). Consequently, central CaTs have a slower rise time, a delayed peak and are smaller in amplitude.

The scarcity of t-tubules in atrial cells also affects beat-to-beat Ca^{2+} removal that occurs through reuptake into the SR by SERCA and extrusion across

the sarcolemma predominantly via Na^+–Ca^{2+} exchange (NCX). In atrial myocytes Ca^{2+} released from nj-SR CRUs occurs at greater distances from NCX and therefore the contribution of NCX to beat-to-beat Ca^{2+} removal is likely to differ from ventricular cells. Furthermore, increased NCX activity is a hallmark of myocytes from failing hearts and the electrogenic nature of its activity as cause for arrhythmogenic disturbances in ventricular tissue is well established (Pogwizd *et al.* 1999); however, the role of NCX in atrial arrythmogenesis still needs to be determined.

Atrial myocytes are also unique compared to ventricular cells in their significantly higher expression levels of a second type of SR Ca^{2+} release channel, the inositol-1,4,5-trisphosphate receptor (IP_3R; Lipp *et al.* 2000). IP_3Rs are part of a G_q-protein coupled receptor (GPCR) signalling pathway and release Ca^{2+} from the SR upon binding of IP_3 in a $[Ca^{2+}]_i$-dependent fashion. IP_3R-induced Ca^{2+} release (IICR) has been hypothesized to lower the threshold for the activation of RyRs by CICR and may directly contribute to Ca^{2+} transients (Kockskamper *et al.* 2008). In cardiac disease such as hypertrophy, HF (Wang *et al.* 2003) and atrial fibrillation (Yamda *et al.* 2001) IP_3R expression levels are further increased. Furthermore, patients with cardiac hypertrophy or HF have elevated levels of Angiotensin II (Ang II; Nattel, 2002), a hormone that binds to GPCRs and exerts its effect, at least in part, by enhancing IICR. Taken together, evidence is growing that IP_3R-mediated Ca^{2+} signalling plays a critical role in cardiac disease, but the specific ramifications for atrial function are poorly understood.

Mitochondria contribute to Ca^{2+} cycling during ECC at different levels, from providing the fuel (ATP) for ion pumps (including SERCA) and substrate for phosphorylation of Ca^{2+} handling proteins, to control of the redox environment and to Ca^{2+} buffering (Dedkova & Blatter, 2012, 2013). While it is generally agreed that mitochondria are capable of sequestering Ca^{2+}, even in large quantities, it has remained controversial whether significant amounts of Ca^{2+} buffering can occur during ECC on a beat-to-beat basis and thus whether mitochondria can shape the CaT in space and time (Bootman *et al.* 2006; O'Rourke & Blatter, 2009; Dedkova & Blatter, 2013). Again, the scarcity of t-tubules and the spatially inhomogeneous patterns of Ca^{2+} release in atrial cells, raise the question of a specific role of mitochondria for the propagation of activation, and specifically, whether the high density of mitochondria (Barth *et al.* 1992; Mackenzie *et al.* 2004; Hohendanner *et al.* 2013) can impede the propagation of Ca^{2+} release through the network of the nj-SR, and whether this changes in HF.

The goal of this study was a comprehensive characterization of atrial Ca^{2+} cycling during ECC in single myocytes from normal and from failing hearts. We focused on the interplay between IICR, mitochondrial Ca^{2+} buffering and altered NCX activity and its consequences for atrial arrhythmogenesis in HF. We found that in HF enhanced IICR and reduced mitochondrial Ca^{2+} uptake had positive inotropic effects mediated by enhanced CaTs during ECC, but also led to a higher propensity of spontaneous proarrhythmic Ca^{2+} release mediated by enhanced NCX activity.

Methods

Ethical approval

All protocols were approved by the Institutional Animal Care and Use Committee of Rush University Chicago, and comply with US and UK regulations on animal experimentation (Drummond, 2009).

Myocyte isolation and HF induction

Left atrial and left ventricular myocytes were isolated from male New Zealand White rabbits (Myrtle's Rabbitry, Thompsons Station, TN, USA). Rabbits were killed by intravenous injection of pentobarbital sodium (100 mg kg^{-1}). Hearts were excised, mounted on a Langendorff apparatus, and retrogradely perfused with nominally Ca^{2+}-free Tyrode solution for 5 min followed by minimal essential medium Eagle (MEM) solution containing 20 μM Ca^{2+} and 22.5 μg ml^{-1} Liberase Blendzyme TH (Roche Applied Science, Indianapolis, IN, USA) for 20 min at 37°C. The left atrium was removed from the heart and digested for an additional 5 min in the enzyme solution at 37°C. Ventricular or atrial tissue was minced, filtered, and washed in MEM solution containing 50 μM Ca^{2+} and 10 mg ml^{-1} BSA. Isolated cells ($n = 69$ normal hearts) were kept in MEM solution with 50 μM Ca^{2+} at room temperature (20–24°C) until indicator dye loading and subsequent experimentation or cultured and used for experimentation after 24–48 h.

In addition, left atrial and ventricular myocytes were isolated from male rabbits with non-ischaemic HF ($n = 17$ hearts) induced by combined volume and pressure overload. Rabbits underwent two survival surgeries. Volume overload was induced by creation of aortic valve insufficiency, followed 2–4 weeks later by induction of pressure overload by abdominal aorta banding. Surgeries were conducted under isoflurane inhalation anaesthesia after ketamine–xylazine–acepromazine premedication. HF developed gradually (over 5–8 months, monitored by serial echocardiography), and was characterized by depressed systolic ventricular function, and arrhythmogenesis in an animal that has human-like Ca^{2+} handling and elecrophysiological properties (Pogwizd, 1995). Atrial cells were isolated from hearts that showed marked left ventricular dilatation (54 ± 5% increase in left ventricular diastolic internal dimension) and systolic dysfunction (decrease of left ventricular

fractional shortening by 37 ± 4%). Ventricular cells from this model have been studied extensively and are well characterized at structural, biochemical, molecular, Ca^{2+} handling, and electrophysiological levels (Pogwizd, 1995; Pogwizd *et al.* 2001; Bers *et al.* 2002; Despa *et al.* 2002; Shannon *et al.* 2003; Domeier *et al.* 2009; Zima *et al.* 2010).

Cell culture and adenoviral gene transfer

For adenoviral transfections myocytes were kept in short-term culture (≤48 h) using Corning cellgro Medium 199 (VWR, Radnor, PA, USA) supplemented with penicillin and streptomycin (50 μg ml^{-1}). The medium was changed daily. Adenoviral gene transfer (multiplicity of infection of 500) was used to express FIRE1-cyt (fluorescent IP_3 responsive element 1 targeted to the cytosol; Remus *et al.* 2006), an IP_3 affinity trap (Domeier *et al.* 2008), mouse 43 kDa inositol polyphosphate 5′-phosphatase (m43 phosphatase; Kapoor *et al.* 2014), GFP or Mitycam (Kettlewell *et al.* 2009). Experiments were performed after 24 h culture for FIRE1-cyt, IP_3 affinity trap, m43 phosphatase and GFP, and after 48 h culture for Mitycam.

Solutions and chemicals

All chemicals were obtained from Sigma-Aldrich (St Louis, MO, USA) unless noted otherwise. SEA-0400 was obtained from ChemScene (Monmouth Junction, NJ, USA). Fluorescent calcium indicator dyes and MitoTracker Red FM were obtained from Molecular Probes/Life Technologies (Grand Island, NY, USA). Tyrode solution contained (in mM): 130 NaCl, 4 KCl, 2 or 7 $CaCl_2$ (as indicated), 1 $MgCl_2$, 10 D-glucose, 10 Hepes; pH 7.4 (adjusted with NaOH). For experiments on permeabilized myocytes saponin (0.01%) was used for cell membrane permeabilization and cells were kept in an 'internal solution' containing (in mM): 100 potassium aspartate, 15 KCl, 5 KH_2PO_4, 5 MgATP, 0.35 EGTA, 0.067 $CaCl_2$, 0.75 $MgCl_2$, 10 phosphocreatine, and 10 Hepes with 5 U ml^{-1} creatine phosphokinase and 4% dextran (molecular weight: 40000); pH 7.2 (adjusted with KOH). Free $[Ca^{2+}]_i$ and $[Mg^{2+}]_i$ of this solution were 150 nM and 1 mM, respectively (calculated using Maxchelator, Stanford University). All cells were plated on laminin-coated glass coverslips and superfused with 2 mM Ca^{2+} Tyrode solution. To prevent movement of cells during confocal imaging blebbistatin (10 μM; Tocris Bioscience, Bristol, UK) was added to all Tyrode based solutions. 'Mitochondrial solution' contained (in mM): 135 KCl, 5 NaCl, 20 Hepes, 5 pyruvate, 2 glutamic acid, 2 malic acid, 0.5 KH_2PO_4, 1 $MgCl_2$, 5 EGTA, 15 BDM. Free $[Ca^{2+}]$ of this solution was set to 0 or 5 μM by addition of $CaCl_2$ (as determined with Maxchelator).

$[Ca^{2+}]_i$ and $[Ca^{2+}]_{SR}$ measurements

Indo-1 AM (5 μM, loading for 30 min at room temperature, followed by 15 min wash) was used to ratiometrically (excitation at 360 nm, emission collected at 405 (F_{405}) and 485 (F_{485}) nm) measure averaged whole-cell $[Ca^{2+}]_i$. Background signals were subtracted and $[Ca^{2+}]_i$ changes are expressed as the ratio $R = F_{405}/F_{485}$. Fluo-4 and Fluo-5N were used for confocal cytosolic and SR $[Ca^{2+}]$ measurements. Changes in $[Ca^{2+}]$ measured with single wavelength dyes are expressed as F/F_0 where F_0 refers to resting fluorescence in unstimulated cells measured at the begin of an experiment or diastolic fluorescence levels measured under control steady-state conditions during electrical stimulation, respectively. CaT amplitudes were quantified as $\Delta F/F_0$ and ΔR, respectively, where $\Delta F = F - F_0$ and $\Delta R = R_{peak} - R_{diast}$. For confocal $[Ca^{2+}]_i$ measurements cells were loaded with Fluo-4 AM (5 μM, excitation at 488 nm, emission at 515 nm) for 20 min. For $[Ca^{2+}]_{SR}$ measurements cells were loaded with Fluo-5N AM (10 μM, excitation at 488 nm, emission at 515 nm) for 1 h 45 min. All dye loading procedures were followed by a washing period (>10 min) in Tyrode solution. Confocal line scan images were recorded at 512 lines s^{-1} using a ×60 oil-immersion objective lens (NA = 1.49) with a Nikon A1R system (Nikon Corporation, Melville, NY, USA). The scan line was placed along the longitudinal or transversal axis (as indicated) of the cell using pixel dimensions of 0.03–0.24 μm. Subcellular CaTs reflecting Ca^{2+} release from j-SR (SS, subsarcolemmal) and nj-SR (CT, central) were derived from 1 μm wide regions. The centripetal propagation velocity of CICR in atrial myocytes was derived from transverse confocal line scan images and calculated as the distance between two subcellular locations of interest and the interval between the times when the local CaTs reached half-maximal amplitude at these respective locations. The empirically measured point-spread function of the system had full width at half-maximum (FWHM) values of 0.28, 0.29 and 0.7 μm in the x, y and z (axial) dimensions (Maxwell & Blatter, 2012). Action potentials and global CaTs were elicited by electrical field stimulation (0.5 Hz) of intact atrial myocytes using a pair of platinum electrodes (voltage set at 50% above the threshold for contraction). Caffeine (10 mM) was used to deplete SR Ca^{2+} stores and measure the SR Ca^{2+} content. Experiments were conducted at room temperature (20–24°C).

IP_3 and IICR

A cytosol-targeted FRET-based IP_3 biosensor (FIRE1-cyt; for a detailed description see Remus *et al.* 2006) was used to dynamically study $[IP_3]_i$ in atrial cells. Briefly, FIRE1-cyt reports fluorescence resonance energy transfer (FRET) between cyan and yellow fluorescent protein (CFP and

YFP) upon binding of IP_3. FIRE1-cyt is a fusion protein of the IP_3 binding domain of the IP_3 receptor type 1 with CFP and YFP at the amino and carboxyl termini, respectively. Upon excitation of CFP at 457 nm, an increase in $[IP_3]$ leads to increased FRET and a detectable change in the YFP/CFP fluorescence ratio (emissions were measured at >530 and 488 nm).

Inhibition of IICR was achieved by (i) adenoviral expression of FIRE1-cyt lacking CFP and YFP sequences which acts as a buffer of cytosolic IP_3 (IP_3 affinity trap; Domeier *et al.* 2008); (ii) adenoviral transfer of mouse inositol polyphosphate 5′ phosphatase (m43; Kapoor *et al.* 2014) which rapidly and efficiently degrades the biologically active IP_3 by removing the 5′ phosphate (Majerus *et al.* 1999; Vasilevski *et al.* 2008); and (iii) application (5 min) of the IP_3R blocker 2-aminoethoxydiphenyl borate (2-APB, 10 μM).

Elevation of $[IP_3]_i$ in intact myocytes was achieved by agonist stimulation with angiotensin II (Ang II; 0.25 μM in freshly isolated myocytes; 10 μM in cultured cells) or by photolysis of caged IP_3 (cag-IP_3 PM; SiChem, Bremen, Germany). Cells were loaded with 100 nM cag-IP_3 for 20 min, and liberation of biologically active IP_3 was achieved by 405 nm laser illumination in user-defined cellular regions using the Mosaic illumination tool integrated in the Nikon A1R confocal imaging system (Shkryl *et al.* 2011).

Elementary IP_3R-mediated Ca^{2+} release events (Ca^{2+} puffs) were recorded in permeabilized atrial cells after stimulation with IP_3 (D-*myo*-inositol 1,4,5-trisphosphate, hexapotassium salt; Tocris Bioscience, Bristol, UK) and inhibition of RyR-mediated Ca^{2+} release with tetracaine (4 mM; 'Ca^{2+} puff protocol'; Zima & Blatter, 2004).

Mitochondria

Cultured (48 h) left atrial myocytes were adenovirally transfected with the mitochondria-targeted fluorescent Ca^{2+} probe Mitycam (Kettlewell *et al.* 2009) to measure mitochondrial distribution and density as well as mitochondrial Ca^{2+} uptake. Mitycam is an inverse pericam that is excited at 488 nm and emission is measured at 530 ± 15 nm. Changes of $[Ca^{2+}]_{mito}$ are expressed as $1-(F/F_0)$. For structural studies (density and distribution of mitochondria) with Mitycam or MitoTracker Red FM (25 μM, 30 min loading at 37°C, excitation at 543 nm, emission at >600 nm) atrial cardiomyocytes were kept in Tyrode solution and two-dimensional (2D) confocal images were recorded from a central plane. Mitochondrial Ca^{2+} uptake via mitochondrial Ca^{2+} uniporter (MCU) was studied in permeabilized cells expressing Mitycam. For the inhibition of the MCU, the ruthenium compound Ru360 (10 μM, EMD Chemicals, Philadelphia, PA, USA) was used.

Data analysis and statistics

The Liscana algorithm (Hohendanner *et al.* 2013) was used to analyse mitochondrial density and cell area.

The frequency of Ca^{2+} puffs and the frequency, amplitude, spatial width (FWHM), full duration (full duration at half-maximum, FDHM) and time to peak (TTP) of Ca^{2+} sparks were analysed with SparkMaster (Picht *et al.* 2007). Because of the small amplitude of the signal, Ca^{2+} puff amplitude, FWHM, FDHM and TTP were further verified by manual analysis.

The relative contribution of NCX to Ca^{2+} removal during CaTs (referred to as 'NCX activity') was calculated as:

$$\text{NCX activity}=[1-(1/\tau_{CaT}-1/\tau_{Caffeine})]/[1/\tau_{CaT}] \quad (1)$$

where the time constants τ_{CaT} and $\tau_{Caffeine}$ were obtained by mono-exponential fits to the decay of electrically and caffeine-evoked CaTs in the same cell. The assay is based on the notion that the decline of an AP-induced CaT results from Ca^{2+} extrusion via NCX *and* reuptake into the SR via SERCA pump, whereas during caffeine (10 mM) exposure $[Ca^{2+}]_i$ declines solely by NCX extrusion. By considering the time constants τ_{CaT} and $\tau_{Caffeine}$ (cf. Fig. 7*Ea*) according to eqn (1) a measure of NCX activity can be derived that estimates the percentage contribution of NCX to the decline of an electrically evoked CaT.

Statistical comparisons were made using Student's *t* test or one-way ANOVA for paired or unpaired data, with statistical significance set at $P < 0.05$. Data are presented as individual observations or as means ± SEM of n measurements, where n is the number of cells.

Results

Ca^{2+} transients and SR Ca^{2+} depletion during ECC in normal and HF myocytes

We compared cytosolic CaTs between left atrial myocytes from normal rabbits and rabbits with systolic heart failure (Maxwell *et al.* 2012). Cytosolic CaTs were elicited by electrical field stimulation and recorded with Fluo-4 by line scan confocal imaging (Fig. 1*Aa* and *d*). As expected for a cardiac cell type lacking transverse tubules (Huser *et al.* 1996; Kockskamper *et al.* 2001) $[Ca^{2+}]_i$ rose first and to the highest level in the cell periphery (SS in Fig. 1*Aa*, corresponding to Ca^{2+} release from j-SR), followed by propagation of Ca^{2+} release in centripetal direction where $[Ca^{2+}]_i$ peaked with a delay at significantly (Fig. 1*Ab* and *C*) lower levels (CT in Fig. 1*Aa*, corresponding to Ca^{2+} release from nj-SR). In atrial cells

from failing hearts, CaTs were prolonged and significantly higher in amplitude in central regions of the cell (Fig. 1*Ae* and *C*). This is in stark contrast to ventricular myocytes where CaTs were significantly depressed in HF (Fig. 1*Af* and *E*) compared to normal myocytes (Fig. 1*Ac* and *E*). Furthermore, the centripetal propagation velocity of Ca^{2+} release was significantly accelerated in atrial HF myocytes (Fig. 1*D*; HF: $205 \pm 19\ \mu m\ s^{-1}$; normal: $147 \pm 13\ \mu m\ s^{-1}$). Consistent with the larger amplitude of cytosolic CaTs in HF atrial myocytes, the beat-to-beat SR Ca^{2+} depletion transients (Fig. 1*B*) were significantly larger in HF atrial myocytes (Fig. 1*F*).

IICR induced by angiotensin II

Ang II is known to increase $[IP_3]_i$ and to exert a positive inotropic effect in cardiac mycoytes (Meissner *et al.* 1998; Remus *et al.* 2006). Ang II levels as well as Ang II receptor expression on cell surfaces are increased *in vivo* in different models of cardiac disease (e.g. atrial fibrillation; Nattel, 2002); however, Ang II has also been shown to depress left ventricular contractile performance in HF (Cheng *et al.* 1996). We compared the effects of Ang II stimulation on diastolic $[Ca^{2+}]_i$, CaTs and SR Ca^{2+} load in normal and HF atrial myocytes. CaTs were elicited by field stimulation

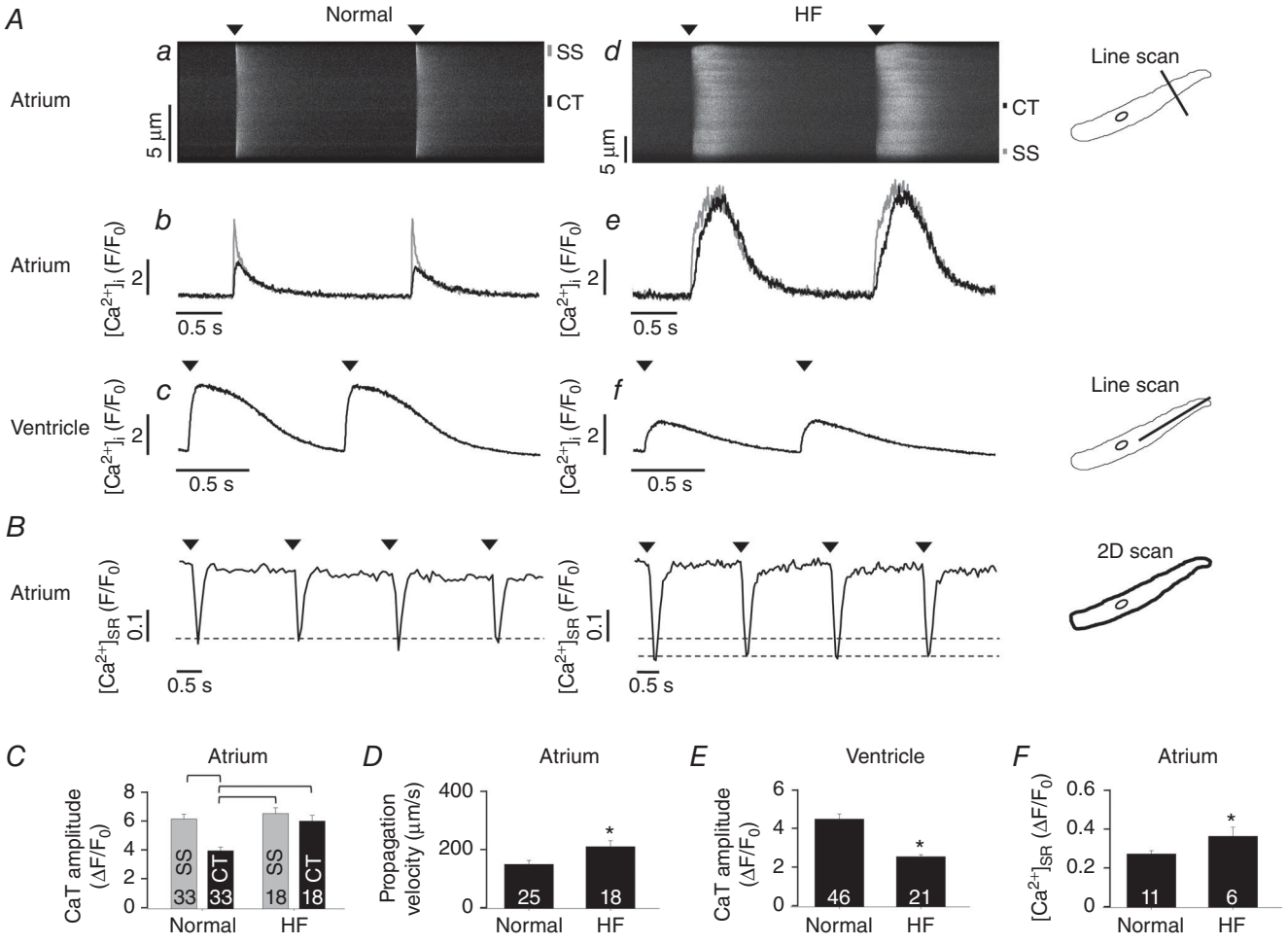

Figure 1. Ca^{2+} cycling during ECC in normal and HF left atrial myocytes
A, control line scan images (*a*, *d*) and CaTs (*b*, *e*) from central (CT) and subsarcolemmal (SS) cytosolic regions of normal and HF atrial myocytes and from control (*c*) and HF (*f*) ventricular cells. Arrowheads indicate electrical stimulation. *B*, $[Ca^{2+}]_{SR}$ traces obtained from whole-cell imaging of Fluo-5 N fluorescence in normal (left) and HF (right) atrial myocytes. Arrowheads indicate electrical stimulation. *C*, summary data of local CaT amplitudes in CT and SS regions of normal and HF atrial myocytes obtained from transversal line scans. Square brackets indicate significant differences at $P < 0.05$, one-way ANOVA. *D*, summary data for the centripetal Ca^{2+} propagation velocity in normal and HF atrial cells derived from transversal line scans. *E*, summary data for the CaT amplitude in normal and HF ventricular myocytes obtained from longitudinal line scans. *F*, summary data for the $[Ca^{2+}]_{SR}$ depletion amplitude in normal and HF atrial myocytes as obtained from 2D confocal measurements of Fluo-5 N fluorescence. Panels *D*–*F*: $^*P < 0.05$, Student's *t* test. Here and subsequent figures: numbers in bar graphs indicate n = number of cells.

and in each experiment SR Ca^{2+} load was estimated from the amplitude of the $[Ca^{2+}]_i$ signal elicited by rapid application of caffeine (10 mM; Fig. 2*A*). We confirmed the Ang II-dependent intracellular IP_3 production using the FRET-based IP_3 biosensor FIRE1-cyt (Remus *et al.* 2006). As shown in Fig. 2*B*, Ang II stimulation increased $[IP_3]_i$ significantly in normal and HF atrial myocytes, but there was no difference in magnitude of this increase between normal and HF cells, although the sensitivity and dynamic range of the IP_3 biosensor may not be sufficient to detect these potentially small changes (Fig. 2*F*). In atrial myocytes from failing hearts, diastolic $[Ca^{2+}]_i$ levels, measured ratiometrically with Indo-1, were significantly increased compared to normal cells (Fig. 2*C*), and treatment with Ang II increased diastolic $[Ca^{2+}]_i$ in normal and HF myocytes even further. The whole-cell CaT amplitudes measured with Indo-1, were significantly increased in HF cells (+32%; Fig. 2*A* and *D*), thus confirming the results obtained with Fluo-4 (Fig. 1*C*). However, Ang II significantly *decreased* the CaT amplitude in HF cells by 36% (Fig. 2*D*, $P < 0.05$). Additionally, the SR Ca^{2+} content was unchanged in HF atrial cells compared to normal cells. However, exposure of cells to Ang II for >5 min decreased the SR Ca^{2+} load significantly in HF, whereas it had no effect in normal atrial cells (Fig. 2*E*).

IICR induced by cytosolic uncaging of IP_3

To further elucidate the role of IP_3R-mediated Ca^{2+} release during ECC in normal and HF atrial myocytes, we loaded atrial myocytes with the caged IP_3 compound cag-IP_3.

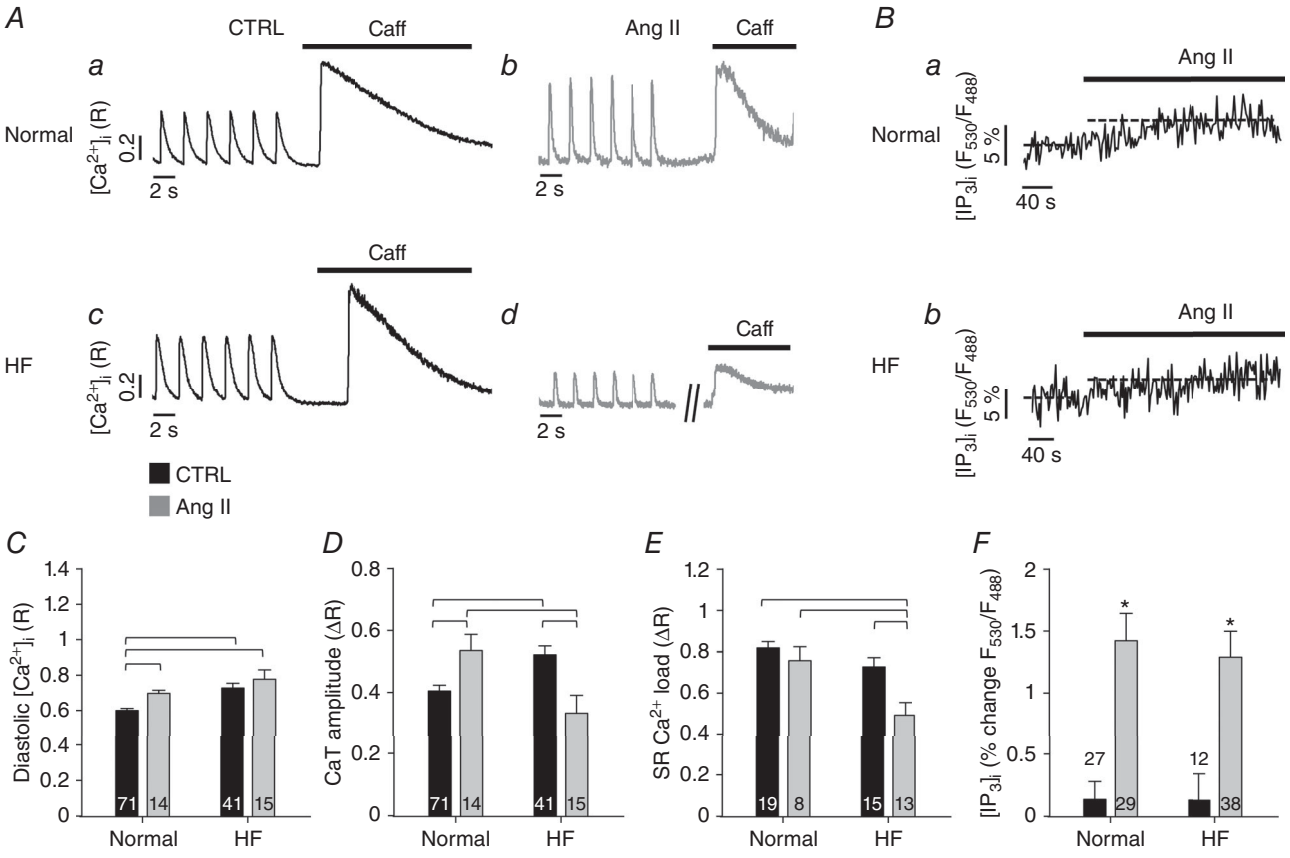

Figure 2. Effect of Ang II on Ca^{2+} signalling during ECC in atrial cells
A, electrically and caffeine-evoked CaTs in normal (top) and HF (bottom) atrial cells before (*a*, *c*; CTRL) and after (*b*, *d*) application of Ang II. *B*, changes of $[IP_3]_i$ in normal (*a*) and HF (*b*) atrial myocytes revealed by measurement of FRET between CFP and YFP in cells expressing the IP_3 biosensor FIRE1-cyt. *C*, diastolic $[Ca^{2+}]_i$ during field stimulation in normal and HF myocytes under control conditions (black) or after treatment with Ang II (grey). *D*, CaT amplitudes during field stimulation in normal and HF myocytes under control conditions (black) or after treatment with Ang II (grey). *E*, SR Ca^{2+} load assessed from changes of $[Ca^{2+}]_i$ induced by rapid application of 10 mM caffeine, in normal and HF myocytes under control conditions (black) or after treatment with Ang II (grey). In panels *C*–*E* square brackets indicate significant differences at $P < 0.05$, one-way ANOVA. *F*, grey bars show average increase of FIRE1-cyt FRET signal (F_{530}/F_{488}) after application of AngII in normal and HF myocytes. Black bars represent changes of control FRET signal over the same time interval in the absence of AngII. *$P < 0.05$, Student's *t* test.

Upon UV-light exposure, cag-IP_3 instantaneously released biologically active IP_3 which led to an increase of $[IP_3]_i$ levels as confirmed by FIRE1-cyt measurements (Fig. 3*A* and *B*). Global IP_3 uncaging significantly increased the CaT amplitude in regions of the nj-SR (CT in Fig. 3*C*) in normal atrial cells with little effect on SS CaTs. In HF atrial myocytes, however, IP_3 uncaging led to a similar decrease of Ca release from j-SR and nj-SR (Fig. 3*E*). This decrease in CaT amplitude in HF myocytes was due to a combined effect of reduced peak CaT (by 17 ± 2 and 19 ± 3% in CT and SS regions) and an increase in diastolic $[Ca^{2+}]_i$ (by 57 ± 7 and 70 ± 8% in CT and SS regions). Averaged over the entire cells the increase in diastolic $[Ca^{2+}]_i$ 20 s after IP_3 uncaging was almost twice as large in HF as in normal cells ($[Ca^{2+}]_{diast}$ (F/F_0): 1.36 ± 0.06 in normal cells ($n = 12$); 1.67 ± 0.13 in HF cells ($n = 6$); $P < 0.05$). The IP_3R blocker 2-APB (10 μM) abolished the IP_3 effects (Fig. 3*D*), confirming that the observed effects on CaT amplitude were mediated by IICR, and actually decreased CaT amplitudes below control levels, suggesting that basal IP_3 activity made a contribution towards the magnitude of CaTs under control conditions.

Effect of basal $[IP_3]_i$ on CaTs

We investigated the effect of basal IP_3 activity on CaTs further, using three different methodological approaches.

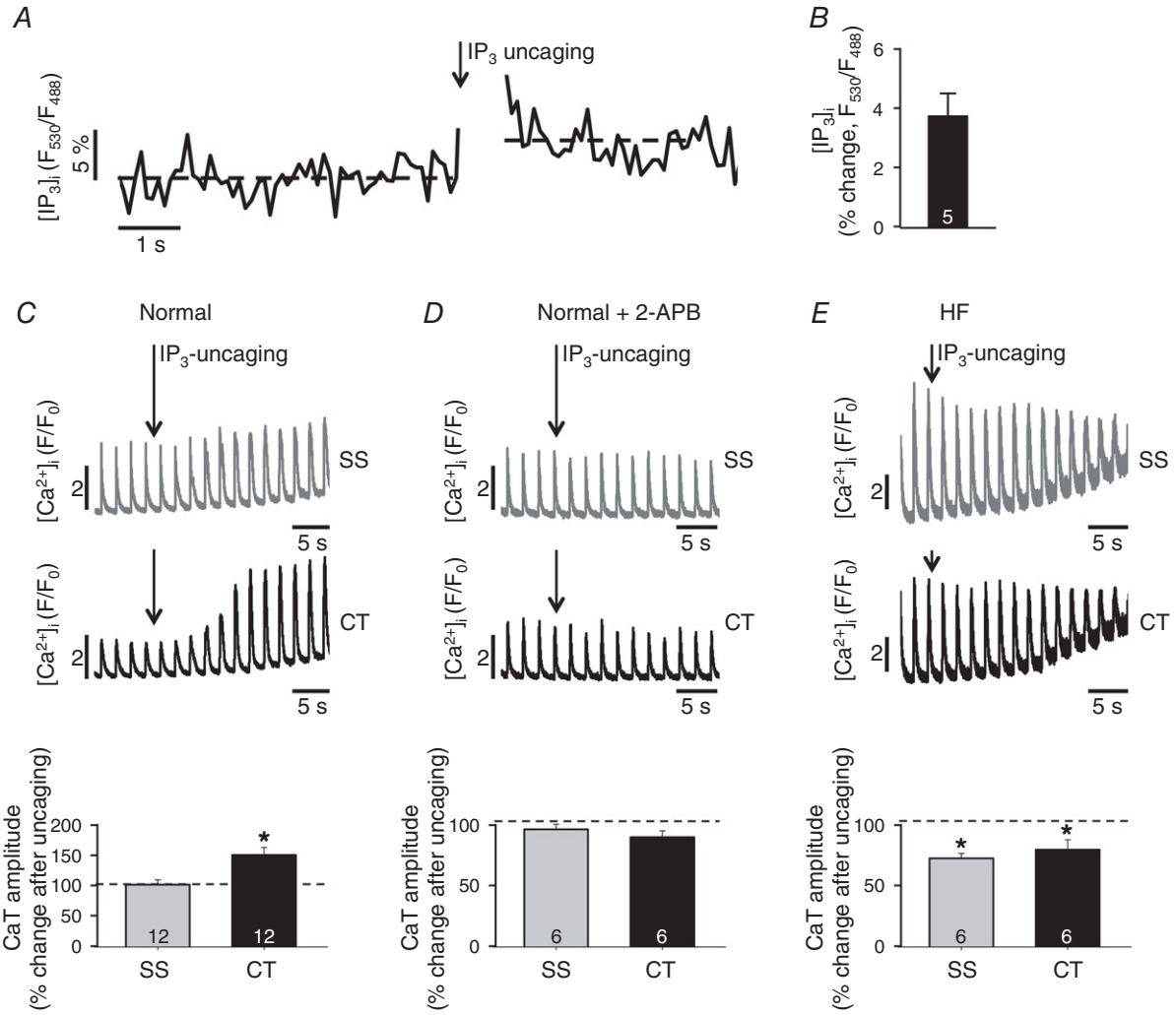

Figure 3. Effect of IP_3 uncaging on Ca^{2+} signalling during ECC in atrial cells
A, change of $[IP_3]_i$ in an atrial myocyte expressing FIRE1-cyt before and after IP_3 uncaging. *B*, average percentage change of the $[IP_3]_i$-dependent FIRE1-cyt FRET signal (F_{530}/F_{488}) averaged over 3 s after uncaging. *C* and *E*, effect of global whole-cell IP_3 uncaging on local CaTs in the subsarcolemmal (SS) and central (CT) cytosol in normal (*C*) and HF (*E*) atrial myocytes. *D*, same experiment as in panel *C* but in the presence of the IP_3R blocker 2-APB. Panels *C*–*E*, bottom: summary data of IP_3 uncaging effects on CaT amplitudes. *$P < 0.05$, Student's *t* test. 100% corresponds to the average $[Ca^{2+}]_i$ levels before IP_3 uncaging.

First, we used the pharmacological IP_3R blocker 2-APB. In the presence of 2-APB the CaT amplitude was reduced in atrial myocytes; however, this basal IP_3 effect was significantly more pronounced in HF (Fig. 4*E*; cf. also Fig. 3*D*). In two additional series of experiments we adenovirally expressed the IP_3 binding domain of the IP_3R type 1 (IP_3 affinity trap) or the m43 phosphatase in the cytosol. Both strategies aimed to reduce $[IP_3]_i$ levels. As a control we transfected cells with an adenovirus encoding GFP and determined in control measurements that CaT amplitudes were identical in the presence or absence of the virus (data not shown). Figure 4*Aa* and *Ba* shows CaT in virus infected normal and HF atrial cells. As in uninfected cells (Figs 1 and 2) the CaT amplitude was increased in HF atrial myocytes. In atrial cells expressing the IP_3 affinity trap (Fig. 4*Ab* and *Bb*) or m43 phosphatase (Fig. 4*Ac* and *Bc*) the CaT amplitude was reduced in normal cells (albeit statistically not significant) and to a significantly larger degree in HF atrial myocytes. For comparison, m43 phosphatase expression in normal ventricular myocytes had no effect on CaT amplitudes, suggesting a lower basal IP_3 activity in ventricular cells. The effect of inhibition of IP_3 signalling with three distinctly different methods yielded extremely consistent results (Fig. 4*C–E*) and validated the use of 2-APB as a valuable tool to inhibit IP_3Rs in cardiac cells. As shown in Fig. 4*F* the effect of basal $[IP_3]_i$ levels on CaT amplitude affected predominantly release of Ca^{2+} from j-SR in normal cells, whereas in HF atrial myocytes the effect was overall more pronounced but affected j-SR and nj-SR to a similar degree.

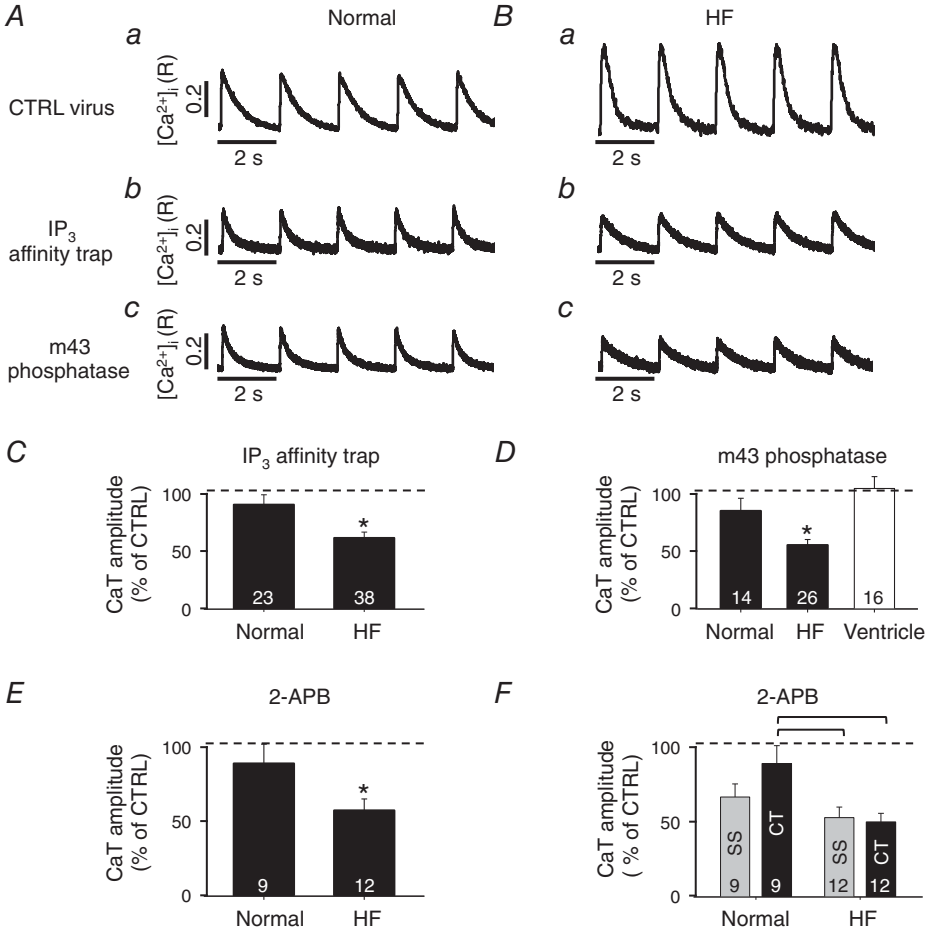

Figure 4. Effect of basal IICR on CaT amplitude
A and *B*, CaTs in field stimulated normal (*A*) and HF (*B*) atrial myocytes after 24 h in culture, expressing a control (CTRL) virus (*a*), IP_3 affinity trap (*b*) or m43 phosphatase (*c*). *C* and *D*, summary data of the percentage change of CaT amplitudes in normal and HF atrial myocytes expressing an IP_3 affinity trap (*C*) or m43 phosphatase (*D*). $^*P < 0.05$ against normal cells, Student's *t* test. In *D*, comparison of m43 phosphatase effect in normal ventricular cells. *E*, summary data of the effect of 2-APB on CaT amplitudes in normal and HF cells. Panels *C–E*: $^*P < 0.05$, Student's *t* test. *F*, same as panel *E* but spatially resolved for the subsarcolemmal (SS) and the central (CT) cytosol. Square brackets indicate significant differences at $P < 0.05$, one-way ANOVA. In panels *C–F*, 100% corresponds to the average CaT amplitudes before inhibition of IP_3 signalling.

Elementary IP_3R-dependent Ca^{2+} release events

Elementary IP_3R-dependent Ca^{2+} release events from clusters of IP_3Rs (termed 'Ca^{2+} puffs', cf. Tovey *et al.* 2001) have been observed in a variety of cell types including atrial myocytes. In cat atrial myocytes their amplitude has been reported to be 70–80% smaller, the duration three to four times longer and the rise time approximately twofold longer than RyR-mediated Ca^{2+} release events (Ca^{2+} sparks; Zima & Blatter, 2004). In order to quantify Ca^{2+} puffs from rabbit atrial myocytes, localized non-propagating elementary Ca^{2+} release events were recorded in permeabilized left atrial myocytes from normal (Fig. 5*A*) and HF hearts (Fig. 5*B*). To abolish RyR-mediated Ca^{2+} release from the SR, the RyR blocker tetracaine (4 mM) was added which resulted in an almost complete cessation of local Ca^{2+} release event activity (Fig. 5*Ab* and *Bb*). For further analysis cells were only included if they displayed no more than 1 event s^{-1} and 100 μm of confocally scanned distance (s^{-1} (100 $\mu m)^{-1}$) in the presence of tetracaine. Cells were subsequently exposed to tetracaine + IP_3 (5 μM) to record elementary Ca^{2+} release events that originated essentially exclusively from IP_3Rs (Fig. 5*Ac* and *Bc*), thus representing Ca^{2+} puffs. In comparison to RyR-mediated Ca^{2+} sparks (Fig. 5*C*), Ca^{2+} puffs recorded in normal (Fig. 5*D*) and HF atrial rabbit myocytes were >50% smaller in amplitude, their duration was more than twofold longer and the rise time of $[Ca^{2+}]_i$ was about 40% longer. The IP_3R origin of Ca^{2+} puffs was confirmed with the cessation of Ca^{2+} release after the addition of 2-APB (Fig. 5*Ad* and *Bd*). The spatio-temporal properties of Ca^{2+} puffs were strikingly similar between normal and HF atrial myocytes: amplitude ($\Delta F/F_0$: 0.38 ± 0.04 in normal cells *vs.* 0.32 ± 0.03 in HF cells), FDHM (62 ± 7 ms normal *vs.* 60 ± 7 ms HF), FWHM (2.7 ± 0.1 μm normal *vs.* 2.7 ± 0.2 HF) and rise time (29 ± 2 ms normal *vs.* 28 ± 2 ms HF). The

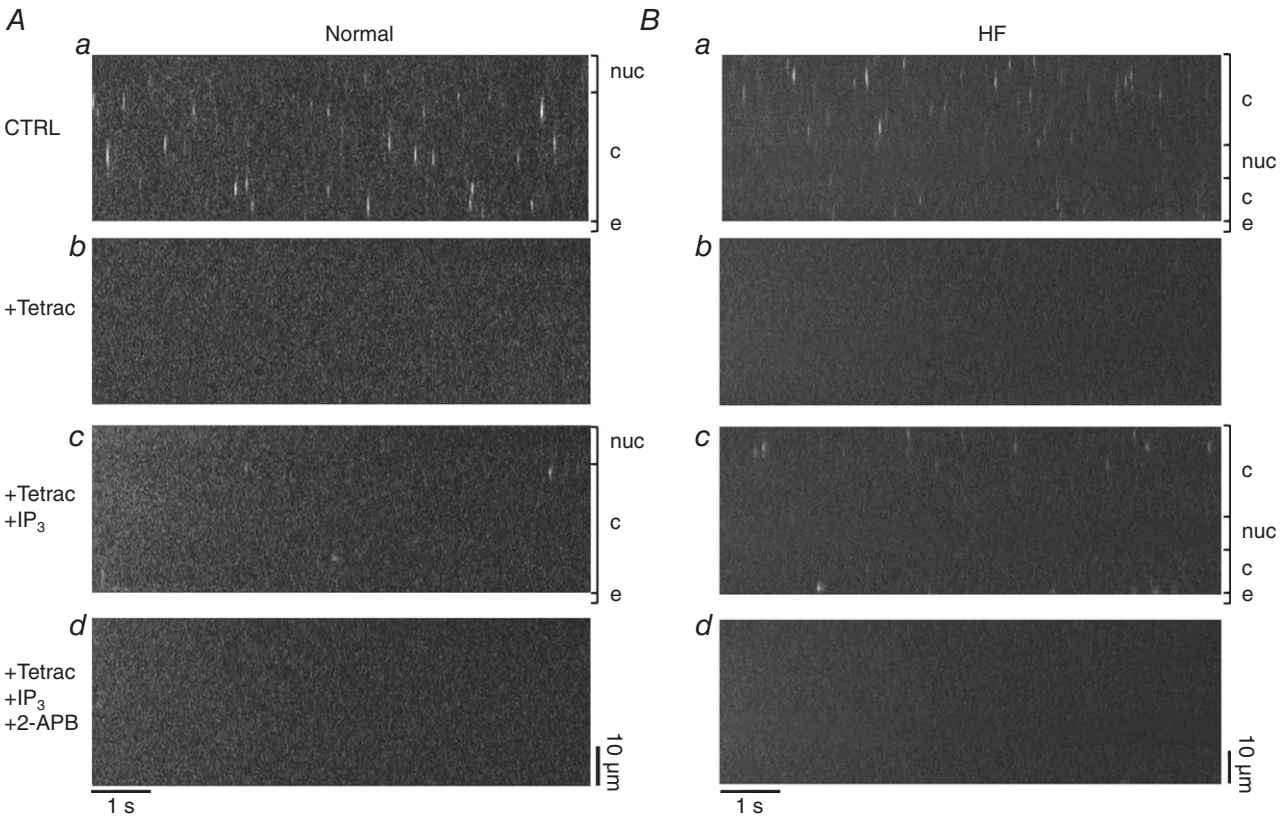

Figure 5. Ca^{2+} puff activity in normal and HF atrial myocytes
A and *B*, examples of longitudinal line scan images from permeabilized normal (*A*) and HF (*B*) myocytes under control (CTRL) conditions (*a*), after application of tetracaine (4 mM) (*b*), tetracaine + IP_3 (5 μM) (*c*), and tetracaine + IP_3 + 2-APB (10 μM) (*d*). nuc, nucleus; c, cytosol; e, extracellular space. *C*, line scan image of a Ca^{2+} spark (top) and Ca^{2+} spark profile (bottom) under control conditions in a normal atrial cell. *D*, line scan image of a Ca^{2+} puff (top) and Ca^{2+} puff profile (bottom) under control conditions in a normal atrial cell. *E*, overall frequencies of Ca^{2+} release events under the four conditions of panels *A* and *B* in normal (black) and HF (grey) cells. *F*, Ca^{2+} puff frequencies in the subsarcolemmal, central cytosolic and perinuclear compartments of normal (black) and HF (grey) atrial cells. Panels *E* and *F*: $^*P < 0.05$, Student's *t* test.

overall frequency of Ca^{2+} puffs was significantly increased in HF (Fig. 5*E*; Ca^{2+} puffs: $0.8 \pm 0.3\ s^{-1}\ (100\ \mu m)^{-1}$ *vs.* $1.8 \pm 0.3\ s^{-1}\ (100\ \mu m)^{-1}$). The subcellular distribution of Ca^{2+} puffs revealed interesting inhomogeneities (Fig. 5*F*). The highest Ca^{2+} puff frequencies were found within a distance of $\leq 2\ \mu m$ from the sarcolemma with no obvious difference between normal and HF myocytes. In contrast, a robust increase in Ca^{2+} puff frequency in HF was found in the central cytosol (Fig. 5*F*; defined as regions with a minimal distance of $2\ \mu m$ to the sarcolemmal or nuclear membrane) which increased from 0.4 ± 0.2 in normal cells to $1.9 \pm 0.3\ Ca^{2+}$ puffs $s^{-1}\ (100\ \mu m)^{-1}$. Interestingly, in normal cells Ca^{2+} puffs were more frequent in the perinuclear region (i.e. at distances $<2\ \mu m$ from the nuclear membrane) compared to the central cytosol; however, in HF myocytes central and perinuclear frequencies were similar. In summary, these results indicate that overall in HF IICR became more prevalent and shifted spatially towards more central regions of the cell, indicative of substantial structural and/or functional remodelling of IP_3-dependent Ca^{2+} signalling in HF.

Effects of mitochondrial Ca^{2+} uptake on Ca^{2+} cycling during ECC

Mitochondria can take up significant amounts of Ca^{2+} and have been shown to influence the spread of activation of Ca^{2+} release during ECC in rat atrial myocytes (Mackenzie *et al.* 2004). This was confirmed here for rabbit atrial myocytes. In cells exposed to the MCU blocker Ru360 CaT amplitudes were increased, but no significant effects on diastolic $[Ca^{2+}]_i$ and SR Ca^{2+} load were observed (Fig. 6*A*). These results suggest that mitochondrial Ca^{2+} uptake can contribute to $[Ca^{2+}]_i$ regulation on a beat-to-beat basis.

Since changes in mitochondrial density in ventricular cells associate with cardiac disease – whereby both, increases and decreases have been reported (Coleman *et al.* 1987; Barth *et al.* 1992; Hohendanner *et al.* 2013) – we measured mitochondrial density in rabbit atrial myocytes. For this purpose we used two different mitochondria-targeted fluorescent probes and measured mitochondrial density in normal and HF atrial

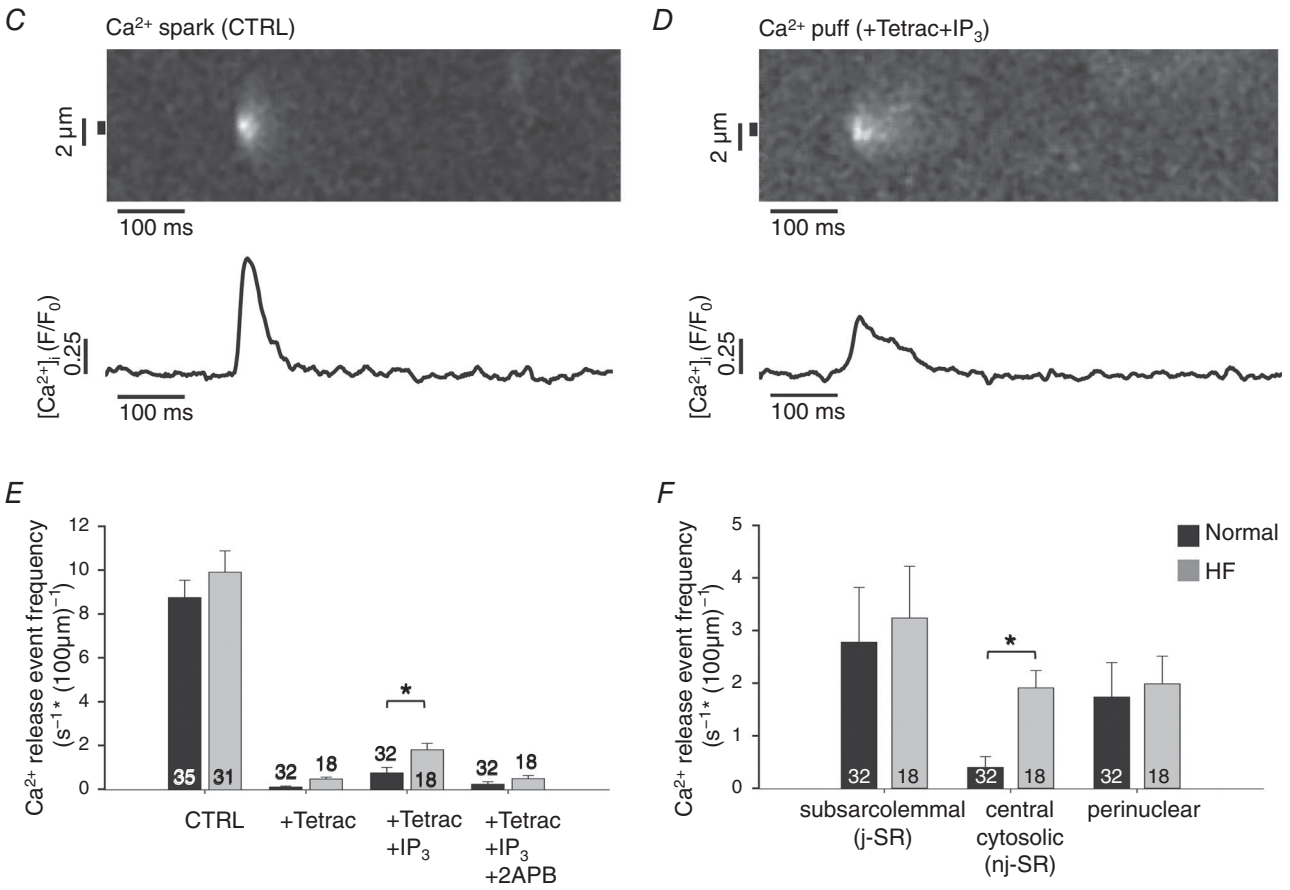

Figure 5. Continued

myocytes. From 2D confocal images of dye-loaded myocytes, binary images were constructed (Fig. 6*B*) that then allowed us to determine the fraction of a cellular cross-section occupied by mitochondria (for details and quantitative evaluation of the algorithm used see Hohendanner *et al.* 2013). Using the probe Mitotracker (Fig. 6*Ca*), HF atrial myocytes revealed a significantly reduced mitochondrial content (estimated cell volume occupied by mitochondria: 33 ± 0.5% in normal cells *vs.* 31 ± 0.7% in HF; $P < 0.05$). Because accumulation of Mitotracker is membrane potential dependent and disease-related potential differences between normal and HF cannot be excluded, we used the fluorescent Ca^{2+}-sensitive mitochondria targeted protein Mitycam (Kettlewell *et al.* 2009) as a second approach to quantify mitochondrial density (Fig. 6*Cb*). Using Mitycam the estimated mitochondrial volume was 38 ± 0.8% in normal and 36 ± 0.7% in HF myocytes ($P < 0.05$). Although the values obtained with Mitycam tended to be higher, both probes reported independently a significantly decreased density of mitochondria in HF. The consequences of reduced mitochondrial density for mitochondrial Ca^{2+} uptake were measured directly using the Mitycam probe. As shown in Fig. 6*D*, exposing Mitycam-loaded mitochondria in permeabilized normal atrial cells to 5 μM extramitochondrial Ca^{2+} resulted in a fast (<1 s) increase of mitochondrial $[Ca^{2+}]$ ($[Ca^{2+}]_{mito}$) that rapidly levelled off; 5 μM is approximately the $[Ca^{2+}]$ for half-maximal activation of the MCU (Sedova *et al.* 2006). In HF atrial myocytes the Ca^{2+} uptake response was blunted. As summarized in Fig. 6*E*, the $[Ca^{2+}]_{mito}$ levels reached in HF cells amounted to only about half of that observed in normal cells, and the uptake kinetics were slowed in HF myocytes. These data indicate that mitochondrial Ca^{2+} uptake occurs on a time scale similar to CaTs and therefore has the potential to buffer Ca^{2+} released during ECC. The reduced mitochondrial density and Ca^{2+} uptake in HF may therefore contribute to the robust increase of the CaT, particularly in the centre of atrial cells (Fig. 1).

Arrhythmogenic spontaneous Ca^{2+} release in HF atrial myocytes

Heart failure patients are significantly more prone to develop atrial fibrillation (Cohn *et al.* 1991; Johnstone

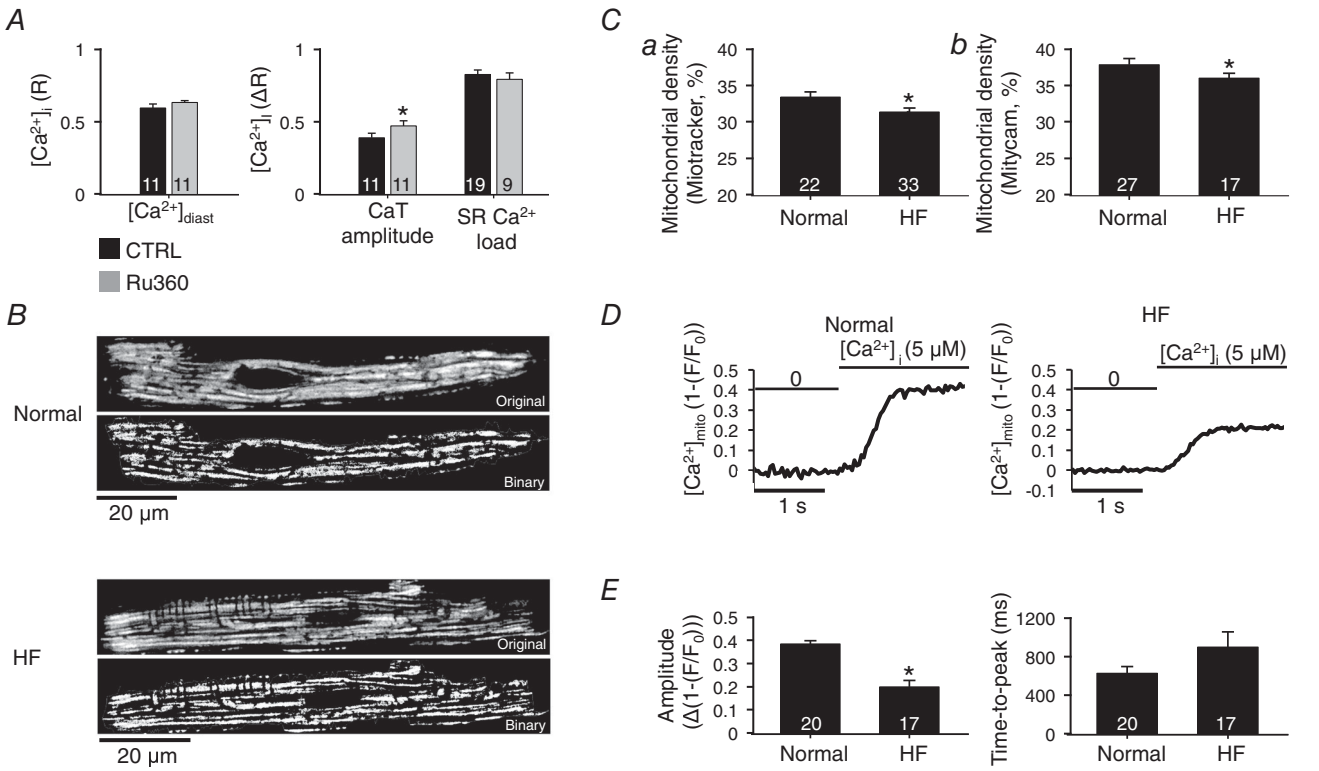

Figure 6. Mitochondrial density and mitochondrial Ca^{2+} uptake
A, average effects of Ru360 on diastolic $[Ca^{2+}]_i$, amplitude of AP-induced CaTs and SR Ca^{2+} load (CaT evoked by 10 mM caffeine). *B*, normal (top) and HF (bottom) atrial cell stained with Mitotracker Red FM. Raw fluorescence images and binary images used to calculate mitochondrial density. *C*, estimated cell volume occupied by mitochondria using Mitotracker (*a*) or Mitycam (*b*). *D*, effect of rapidly increasing $[Ca^{2+}]_i$ from 0 to 5 μM on mitochondrial Ca^{2+} uptake in permeabilized normal and HF atrial cells. *E*, average effect of increasing $[Ca^{2+}]_i$ to 5 μM on amplitude and the time to peak of $[Ca^{2+}]_{mito}$. *$P < 0.05$, Student's *t* test.

et al. 1992; Tsang *et al.* 2002). We therefore tested the hypothesis that in HF atrial myocytes spontaneous pro-arrhythmic Ca^{2+} release events in the form of Ca^{2+} waves occur more frequently, and we explored the effects of spontaneous Ca^{2+} waves on the electrical stability of these cells. Spontaneous Ca^{2+} waves and spontaneous (not electrically triggered) APs were quantified during a 2-min period of rest after >1 min of electrical pacing (arrowheads in Fig. 7*A*) in elevated extracellular Ca^{2+} (7 mM) to facilitate Ca^{2+} loading of the SR (Domeier *et al.* 2012). Spontaneous Ca^{2+} waves were observed in both ventricular (after stimulation at 1 Hz) and atrial (after stimulation at 0.5 Hz) myocytes at frequencies of 0.017 ± 0.003 ($n = 11$) and 0.025 ± 0.005 waves s^{-1}, respectively. (No waves were observed in ventricular cells stimulated at 0.5 Hz). However, the propensity to produce spontaneous waves was significantly increased in HF atrial myocytes. Not only was the fraction of cells revealing waves increased (normal: 75% (30/40 cells); HF: 86% (18/21 cells)), but wave frequency also increased (Fig. 7*Da*: increase to 0.050 ± 0.010 waves s^{-1} in HF) and the latency (the time interval between cessation of pacing and the onset of the first spontaneous Ca^{2+} wave) was reduced from 56 ± 6 s to 32 ± 7 s (Fig. 7*Db*). The spontaneous Ca^{2+} waves in atrial cells revealed a unique spatio-temporal organization. As illustrated in Fig. 7*B*, typically the waves propagated from the site of origin ($t = 0$) along the longitudinal axis of the cell; however, upon closer examination it became evident that in atrial cells the leading wave front propagated through the sub-sarcolemmal space (thus presumably via release of Ca^{2+} from the j-SR) giving rise to a 'U'-shaped wave front ($t = 368$ ms), illustrated in more detail in Fig. 7*C*. Furthermore, 39 ± 7% of all Ca^{2+} waves observed in normal atrial cells and 55 ± 8% of all Ca^{2+} waves in HF atrial cells at some point during propagation induced global Ca^{2+} release, presumably as a consequence of inducing an AP (Fig. 7*Dc*). These events showed the typical $[Ca^{2+}]_i$ pattern of an atrial CaT with an initial ring of elevated $[Ca^{2+}]_i$ in the cell periphery ($t = 385$ ms) that subsequently propagated towards the cell centre ($t = 403$ ms) (Huser *et al.* 1996; Kockskamper *et al.* 2001; Sheehan *et al.* 2006). We will refer to this type of Ca^{2+} wave here as an 'arrhythmogenic Ca^{2+} wave' (arrows in Fig. 7*A*). The overall absolute frequency of arrhythmogenic Ca^{2+} waves was significantly higher in HF atrial myocytes (Fig. 7*Dd*; 0.030 ± 0.007 *vs.* 0.008 ± 0.002 in normal). In contrast to atrial cells, no arrhythmogenic Ca^{2+} waves were observed in ventricular myocytes.

In the next set of experiments we investigated the mechanisms underlying spontaneous and arrhythmogenic Ca^{2+} waves. As shown in Fig. 7*Da* in the presence of the IP_3R blocker 2-APB the frequency of spontaneous Ca^{2+} waves was reduced in atrial myocytes with a more pronounced effect in HF myocytes. In normal cells 2-APB reduced the wave frequency by nearly a third (statistically not significant), whereas in HF the reduction amounted to over half and became statistically significant. Since 2-APB has been reported to potentially also affect Ca^{2+} pumps (Peppiatt *et al.* 2003), we checked for this possibility by assessing the SR Ca^{2+} content with caffeine (10 mM) in normal cells and found no significant difference (amplitude of the caffeine-induced CaT (ΔR): 0.81 ± 0.03 ($n = 19$) control *vs.* 0.75 ± 0.07 ($n = 10$) in 2-APB). The data indicate that basal IP_3-dependent Ca^{2+} signalling facilitated spontaneous SR Ca^{2+} release (Ca^{2+} waves; see also Li *et al.* 2005; Domeier *et al.* 2008), a phenomenon that was more pronounced in HF atrial cells, consistent with enhanced IP_3 activity in HF atrial cells (Figs 2–5).

We further investigated the involvement of NCX in the generation of spontaneous Ca^{2+} waves. The electrogenic nature of NCX action has the potential to depolarize the membrane potential and to initiate Ca^{2+} release. Addition of the NCX inhibitor SEA-0400 (SEA) had no significant effect on the overall Ca^{2+} wave frequency in normal and HF atrial cells. However, NCX inhibition had a very pronounced effect when considering exclusively arrhythmogenic Ca^{2+} waves (Fig. 7*Dc* and *Dd*). SEA significantly reduced the fraction of cells revealing arrhythmogenic Ca^{2+} waves (by 62%) as well as their absolute frequency in normal atrial myocytes, and almost completely abrogated this wave type in HF atrial myocytes, suggesting an enhanced role of NCX for the occurrence of arrhythmogenic Ca^{2+} waves, especially in HF. We quantified NCX activity from the time constants of the decline of electrically (τ_{CaT}) and caffeine ($\tau_{Caffeine}$)-evoked CaTs (Fig. 7*Ea*) as outlined in the Methods section (eqn (1)). The experiments revealed two important results. First, as shown in Fig. 7*Eb*, SEA efficiently reduced NCX activity. Second, in HF atrial cells NCX activity was significantly increased (by 76 ± 30%; $P < 0.05$). The latter results are similar to the increase of NCX activity found in rabbit HF ventricular cells (Bassani *et al.* 1994; Pogwizd *et al.* 1999). Together these data indicate that HF atrial cells have a lower Ca^{2+} wave threshold, are more likely to show spontaneous Ca^{2+} waves and are more prone to develop Ca^{2+} waves with subsequent cell-wide depolarization due to an increased NCX activity compared to normal atrial myocytes.

Discussion

In this study, we investigated IP_3-dependent Ca^{2+} release and its role for ECC in normal atrial cells and atrial myocytes from a left ventricular heart failure model. The key findings of our investigation were as follows: first, in HF atrial myocytes, AP-dependent CaTs were enhanced in amplitude and duration, whereas ventricular CaTs were depressed. Primarily more robust Ca^{2+} release from nj-SR

and faster propagation of activation were responsible for this positive inotropic response. Second, HF atrial myocytes revealed enhanced IICR that preferentially facilitated Ca^{2+} release from central nj-SR and was, at least in part, the cause of enhanced inotropy in HF atrial myocytes. Third, HF atrial myocytes revealed a reduced mitochondrial density that resulted in reduced Ca^{2+} sequestration, with the consequence of larger amplitude CaTs. Finally, HF atrial myocytes revealed a higher propensity of proarrhythmic Ca^{2+} waves that resulted from the combined effect of enhanced IICR and increased NCX activity.

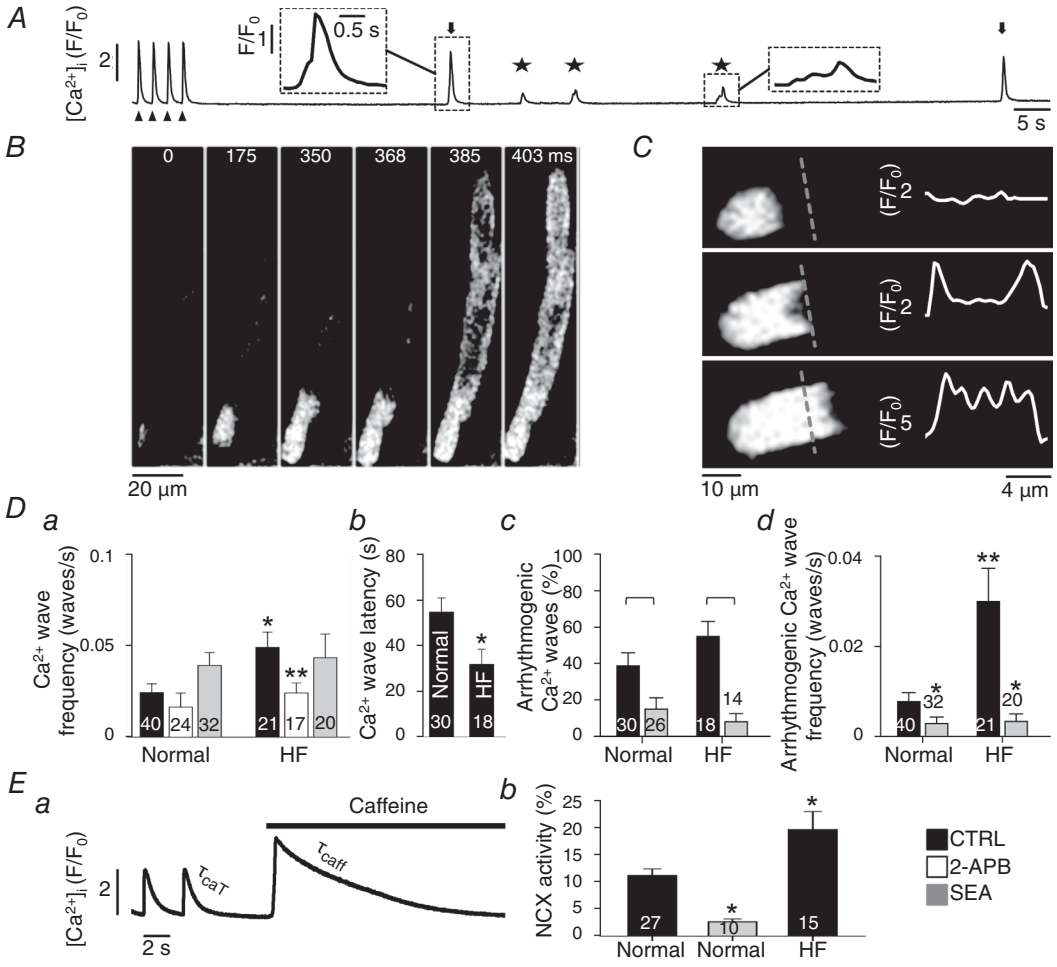

Figure 7. Arrhythmogenic Ca^{2+} waves and NCX activity in normal and HF atrial myocytes
A, protocol to monitor spontaneous Ca^{2+} wave activity. Cells were electrically paced (arrowheads) at 0.5 Hz in 7 mM extracellular [Ca^{2+}] to enhance SR Ca^{2+} loading. Ca^{2+} waves were quantified during a 2-min rest period after cessation of pacing. The stars mark spontaneous Ca^{2+} waves without global cell-wide Ca^{2+} release and arrows mark arrhythmogenic Ca^{2+} waves. *B*, spontaneous Ca^{2+} wave in a single atrial myocyte observed during a rest period after pacing. The Ca^{2+} wave led to subsequent global Ca^{2+} release by triggering an AP and SR Ca^{2+} release typical for atrial ECC ('arrhythmogenic Ca^{2+} wave'). *C*, confocal 2D image from a central focal plane revealing the 'U-shaped' wave front (left) and normalized fluorescence profiles (F/F_0) recorded along the dashed line (right). *Da*, frequency of spontaneous Ca^{2+} waves in normal and HF cells under control (CTRL) conditions (black), after the application of 2-APB (white) and SEA (grey). $^*P < 0.05$ *versus* normal control; $^{**}P < 0.05$ *versus* HF control, Student's *t* test. *Db*, latency of spontaneous Ca^{2+} waves. $^*P < 0.05$, Student's *t* test. *Dc*, fraction of Ca^{2+} waves that induce a spontaneous AP and global CaTs ('arrhythmogenic Ca^{2+} waves') in HF atrial cells before (black) and after application of SEA (grey). In panel *Dc* square brackets indicate significant differences at $P < 0.05$, one-way ANOVA. *Dd*, absolute frequency of arrhythmogenic Ca^{2+} waves in normal and HF atrial myocytes in the absence and presence of SEA. To calculate absolute wave frequencies (panels *a* and *d*), also cells showing no waves were included. $^{**}P < 0.05$ *versus* normal cells in the absence of SEA, Student's *t* test. $^*P < 0.05$ *versus* control, Student's *t* test. *Ea*, protocol used to determine τ_{CaT} and $\tau_{Caffeine}$ for quantification of NCX activity. *Eb*, NCX activity in normal atrial cells (left), after inhibition of NCX in normal atrial cells with SEA, and in HF atrial cells. $^*P < 0.05$ against normal cells, Student's *t* test.

Enhanced IICR in HF: consequences for atrial ECC

Heart failure is characterized by depressed ventricular contractility and arrhythmogenesis. At the cellular level the combination of increased RyR-mediated SR Ca^{2+} leak (Maxwell *et al.* 2012), lower SERCA activity and higher NCX activity (Pogwizd *et al.* 1999), resulting in diminished CaTs and contractility, are hallmarks of systolic HF. The observation of depressed CaTs in single ventricular myocytes presented here (Fig. 1*Af*) confirmed the impaired Ca^{2+} cycling in ventricular myocytes in our rabbit HF model, induced by volume and pressure overload. Patients with systolic heart failure increasingly rely on the atrial contribution to diastolic ventricular filling to maintain cardiac output, but are also more prone to develop atrial fibrillation (AF; Bonow *et al.* 1983; Raymond *et al.* 1998). The irregular rhythm of AF resulting in the loss of the atrial systole and the neurohumoral activation of the renin–angiotensin–aldosterone system due to depressed ventricular contractility are contributing factors to adverse haemodynamic changes (Rahimtoola *et al.* 1975; Linderer *et al.* 1983; Daoud *et al.* 1996; Wijffels *et al.* 1997). Furthermore, atrial (Cao *et al.* 2002; Zhao *et al.* 2007) and ventricular (Go *et al.* 1995; Ai *et al.* 2005) cells show an increase of cytosolic IP_3R expression under conditions of HF and AF. Although IP_3Rs are outnumbered by the much more abundant RyRs by one to two orders of magnitude, they can provide an inotropic reserve by increasing diastolic $[Ca^{2+}]_i$ in the vicinity of the Ca^{2+}-sensitive RyR. This is particularly the case in atrial myocytes that have been shown to express up to six times as many IP_3Rs as ventricular cells (Lipp *et al.* 2000). IICR has been postulated to have positive inotropic effects by sensitizing RyRs and bringing them closer to threshold for activation by Ca^{2+} and to facilitate CICR (Domeier *et al.* 2008; Kockskamper *et al.* 2008; Harzheim *et al.* 2009). Furthermore, Ca^{2+} released through IP_3Rs may contribute directly to systolic CaTs (Foskett *et al.* 2007). A role for IICR directly contributing to systolic CaTs could be explained by the need of IP_3Rs for binding of both Ca^{2+} and IP_3 to release Ca^{2+} from the SR. For 'sensitized' IP_3Rs (with pre-bound IP_3) Ca^{2+} release is expected to be augmented during systolic CaTs, when Ca^{2+} fluxes through LTCC or RyRs are maximal. In our study, photorelease of caged IP_3 or neurohumoral stimulation with Ang II to activate the endogenous IP_3 production confirmed that increased IICR enhanced CaT amplitudes in field-stimulated normal rabbit atrial myocytes. The previously reported upregulation of IP_3Rs in HF and AF (Go *et al.* 1995; Yamda *et al.* 2001; Ai *et al.* 2005) is consistent with our functional results. In HF atrial cells the CaT amplitude was significantly increased, predominantly resulting from enhanced Ca^{2+} release from the central nj-SR. This is consistent with the observed overall increased frequency of elementary Ca^{2+} release events originating from clusters of IP_3Rs (Ca^{2+} puffs) in HF atrial myocytes that was particularly pronounced in areas of the nj-SR. The latter may suggest that the reported increased IP_3R expression in HF is preferentially located to the central cytosolic regions in atrial cells. Interestingly, the spatial and temporal properties of Ca^{2+} puffs were unchanged in HF, only the frequency was increased. This would suggest that IP_3R upregulation in HF may not occur through changes in IP_3R cluster size, but through formation of new clusters that are preferentially located in the nj-SR. This is consistent with the finding that pharmacological IP_3R inhibition (2-APB) predominantly affected j-SR Ca^{2+} release in normal cells whereas j-SR and nj-SR were equally affected in HF atrial cells (Fig. 4*F*).

The notion that IICR significantly contributed to SR Ca^{2+} release during ECC is underscored by the fact that IP_3R inhibition (2-APB), enhanced IP_3 buffering (IP_3 affinity trap) or IP_3 degradation (m43 phosphatase) all decreased the amplitude of CaTs in normal atrial cells and did so even more in HF atrial cells, providing additional experimental support for IICR becoming increasingly more important in HF. The fact that enhancing cytosolic IP_3 degradation by expressing m43 phosphatase had no effect on the CaTs in ventricular cells further underscored the relevance of IP_3 signalling for atrial ECC.

A common finding in patients with developing cardiac hypertrophy and HF is an increased level of Ang II, a hormone that exerts its effects in part by increasing IICR (Li *et al.* 2005; Bootman *et al.* 2007). In our experiments, in normal atrial cells Ang II enhanced Ca^{2+} signalling during ECC, similar to IP_3 uncaging. However, both Ang II and IP_3 uncaging had the opposite effect in HF atrial myocytes. Under steady-state pacing conditions, elevating $[IP_3]_i$ levels decreased the CaT amplitude, an observation that was paralleled by a significant decrease in the SR Ca^{2+} content. Our results, together with the previous observation of enhanced SR Ca^{2+} leak in HF and the sensitivity of Ca^{2+} leak to stimulation of IICR (Zima *et al.* 2010), suggest, that in HF higher IP_3R activity and enhanced IICR ultimately result in Ca^{2+} depletion of the SR. The data suggest that in HF atrial myocytes basal IICR is activated to the extent that it boosts atrial contractility to optimize ventricular filling. However, further stimulation of IP_3 production via humoral pathways (Ang II) or by directly elevating $[IP_3]_i$ (IP_3 uncaging) converts this compensatory positive inotropic effect of IICR into adverse consequences for contractility by depleting the SR of Ca^{2+} and therefore depressing atrial CaTs and subsequently ventricular filling.

Mitochondrial Ca^{2+} uptake

Mitochondria occupy approximately 30% of the cell volume of a cardiac myocyte and play a crucial role in energy metabolism, redox regulation and Ca^{2+}

homeostasis under normal and pathophysiological conditions. Although the question of whether they contribute to Ca^{2+} signalling during ECC on a beat-to-beat basis (O'Rourke & Blatter, 2009) is still a matter of controversy, the organelle is equipped for efficient and rapid Ca^{2+} uptake and release (Wendt-Gallitelli & Isenberg, 1989; Miyata *et al.* 1991; Sedova *et al.* 2006) and is able to buffer significant amounts of Ca^{2+} (Solaro & Briggs, 1974; Dedkova & Blatter, 2012, 2013). Mitochondria further contribute (indirectly) to shaping CaTs by providing ATP to SERCA, influencing RyR activity via ATP-dependent regulation, and generally by setting the redox environment that in turn regulates the activity of Ca^{2+} handling proteins (Zima *et al.* 2013). Mitochondria have been suggested to attenuate the propagation of release through the nj-SR by sequestering cytosolic Ca^{2+} to the extent that mitochondria can act as a 'firewall' against activation of Ca^{2+} release in central regions of atrial myocytes (Mackenzie *et al.* 2004; Bootman *et al.* 2011). When mitochondrial Ca^{2+} uptake was blocked with Ru360 (Matlib *et al.* 1998) in our experiments, CaT amplitudes during ECC were increased without affecting SR Ca^{2+} content. Changes in mitochondrial function and/or structure are of great interest in cardiac disease (Dominic *et al.* 2014). In several disease models increases as well as decreases in mitochondrial density have been reported, suggesting that mitochondrial remodelling in cardiac disease is complex (Coleman *et al.* 1987; Barth *et al.* 1992; Hohendanner *et al.* 2013). We observed a decreased mitochondrial density in HF atrial cells, suggesting a smaller capacity to buffer $[Ca^{2+}]_i$ while the cell size was not significantly increased (1017 ± 50 *vs.* $1255 \pm 118\ \mu m^2$ in normal ($n = 29$) *vs.* HF ($n = 36$) cells; $P = 0.09$). Even though the difference in mitochondrial density between normal and HF atrial myocytes appeared rather small at first glance, the consequences for mitochondrial Ca^{2+} uptake were significant. When testing mitochondrial Ca^{2+} uptake directly, not only was the rate of uptake slowed, the maximum uptake was significantly reduced to approximately half (Fig. 6). Our data suggest that atrial remodelling during HF involves a reduction in mitochondrial density that also turns out to have beneficial effects for ECC. By attenuating mitochondrial Ca^{2+} uptake during ECC, SR Ca^{2+} release became more robust and efficient which ultimately resulted in larger and prolonged CaTs and a positive inotropic effect that would facilitate ventricular filling.

Arrhythmogenic SR Ca^{2+} release in HF

Our data show that HF atrial cells reveal a higher frequency of spontaneous Ca^{2+} waves (Fig. 7). Our experiments indicate that increased IICR plays a critical role. While IP_3R inhibition decreased the Ca^{2+} wave frequency in both normal and HF atrial cells, the effect was significantly more pronounced in HF cells. This is consistent with the upregulation of IP_3 signalling in HF and the more pronounced effect of IICR on electrically evoked CaTs (Fig. 3). In addition, atrial cells in general were prone to develop arrhythmogenic Ca^{2+} waves (around 40% of all Ca^{2+} waves in normal atrial cells), i.e. waves that led to subsequent global Ca^{2+} release by triggering an AP and SR Ca^{2+} release typical for atrial ECC. Arrhythmogenic Ca^{2+} waves were not observed in ventricular cells, thus appear to be a unique feature of atrial cells and occurred more often in HF. This is consistent with findings in atrial cells from hearts with myocardial infarction, where the frequency of spontaneous depolarizations was significantly increased (Kettlewell *et al.* 2013). The spatial propagation pattern of Ca^{2+} waves in atrial cells revealed a unique feature where the front of the propagating wave advanced through the subsarcolemmal space via j-SR Ca^{2+} release, thus preceding the centripetal propagation of CICR from nj-SR. In rabbit atrial cells NCX is exclusively located in the cell periphery due to the lack of transverse tubules. Thus, the subsarcolemmal propagation of the Ca^{2+} wave front exposed NCX for a prolonged period of time to high $[Ca^{2+}]_i$, which might play a critical role in the generation of arrhythmogenic Ca^{2+} waves. Because of the electrogenic nature of NCX, extrusion of elevated $[Ca^{2+}]_i$ will lead to membrane depolarization to the extent that it can trigger an AP. We tested this hypothesis by inhibiting NCX pharmacologically (SEA). NCX inhibition decreased the frequency of arrhythmogenic Ca^{2+} waves significantly in normal atrial cells and did so even more in HF atrial cells, indicating that NCX in forward mode can trigger a depolarization of the cell during spontaneous Ca^{2+} waves. Consistent with our finding of an increased propensity of arrhythmogenic Ca^{2+} waves in HF, NCX activity was indeed enhanced in HF atrial myocytes (Fig. 7*E*).

Conclusions

In hearts with ventricular failure and decreased cardiac output, atrial cells might compensate to maintain ventricular filling despite increased end-diastolic pressure, with a positive inotropic response that results from enhanced atrial CaTs due to increased IICR. The positive inotropic response of atrial cells is aided by reduced Ca^{2+} buffering by mitochondria during ECC. Upregulation of IICR, on the other hand, also has undesirable consequences in form of a significantly higher propensity for arrhythmogenic Ca^{2+} release. The combined action of enhanced IICR together with a higher NCX activity are likely contributors to the arrhythmogenicity found in HF and may form the substrate for the frequently encountered AF in this disease state.

References

Ai X, Curran JW, Shannon TR, Bers DM & Pogwizd SM (2005). Ca^{2+}/calmodulin-dependent protein kinase modulates cardiac ryanodine receptor phosphorylation and sarcoplasmic reticulum Ca^{2+} leak in heart failure. *Circ Res* **97**, 1314–1322.

Alpert JS, Petersen P & Godtfredsen J (1988). Atrial fibrillation: natural history, complications, and management. *Annu Rev Med* **39**, 41–52.

Barth E, Stammler G, Speiser B & Schaper J (1992). Ultrastructural quantitation of mitochondria and myofilaments in cardiac muscle from 10 different animal species including man. *J Mol Cell Cardiol* **24**, 669–681.

Bassani JW, Bassani RA & Bers DM (1994). Relaxation in rabbit and rat cardiac cells: species-dependent differences in cellular mechanisms. *J Physiol* **476**, 279–293.

Bers DM, Pogwizd SM & Schlotthauer K (2002). Upregulated Na/Ca exchange is involved in both contractile dysfunction and arrhythmogenesis in heart failure. *Basic Res Cardiol* **97**(Suppl. 1), I36–42.

Bonow RO, Frederick TM, Bacharach SL, Green MV, Goose PW, Maron BJ & Rosing DR (1983). Atrial systole and left ventricular filling in hypertrophic cardiomyopathy: effect of verapamil. *Am J Cardiol* **51**, 1386–1391.

Bootman MD, Harzheim D, Smyrnias I, Conway SJ & Roderick HL (2007). Temporal changes in atrial EC-coupling during prolonged stimulation with endothelin-1. *Cell Calcium* **42**, 489–501.

Bootman MD, Higazi DR, Coombes S & Roderick HL (2006). Calcium signalling during excitation–contraction coupling in mammalian atrial myocytes. *J Cell Sci* **119**, 3915–3925.

Bootman MD, Smyrnias I, Thul R, Coombes S & Roderick HL (2011). Atrial cardiomyocyte calcium signalling. *Biochim Biophys Acta* **1813**, 922–934.

Cannell MB, Berlin JR & Lederer WJ (1987). Effect of membrane potential changes on the calcium transient in single rat cardiac muscle cells. *Science* **238**, 1419–1423.

Cannell MB & Kong CH (2012). Local control in cardiac E–C coupling. *J Mol Cell Cardiol* **52**, 298–303.

Cao K, Xia X, Shan Q, Chen Z, Chen X & Huang Y (2002). Changes of sarcoplamic reticular Ca^{2+}-ATPase and IP_3-I receptor mRNA expression in patients with atrial fibrillation. *Chin Med J (Engl)* **115**, 664–667.

Chen-Izu Y, McCulle SL, Ward CW, Soeller C, Allen BM, Rabang C, Cannell MB, Balke CW & Izu LT (2006). Three-dimensional distribution of ryanodine receptor clusters in cardiac myocytes. *Biophys J* **91**, 1–13.

Cheng CP, Suzuki M, Ohte N, Ohno M, Wang ZM & Little WC (1996). Altered ventricular and myocyte response to angiotensin II in pacing-induced heart failure. *Circ Res* **78**, 880–892.

Cohn JN, Johnson G, Ziesche S, Cobb F, Francis G, Tristani F, Smith R, Dunkman WB, Loeb H, Wong M *et al.* (1991). A comparison of enalapril with hydralazine-isosorbide dinitrate in the treatment of chronic congestive heart failure. *N Engl J Med* **325**, 303–310.

Coleman R, Silbermann M, Gershon D & Reznick AZ (1987). Giant mitochondria in the myocardium of aging and endurance-trained mice. *Gerontology* **33**, 34–39.

Coombes S & Timofeeva Y (2003). Sparks and waves in a stochastic fire–diffuse–fire model of Ca^{2+} release. *Phys Rev E Stat Nonlin Soft Matter Phys* **68**, 021915.

Daoud EG, Weiss R, Bahu M, Knight BP, Bogun F, Goyal R, Harvey M, Strickberger SA, Man KC & Morady F (1996). Effect of an irregular ventricular rhythm on cardiac output. *Am J Cardiol* **78**, 1433–1436.

Dedkova EN & Blatter LA (2012). Measuring mitochondrial function in intact cardiac myocytes. *J Mol Cell Cardiol* **52**, 48–61.

Dedkova EN & Blatter LA (2013). Calcium signaling in cardiac mitochondria. *J Mol Cell Cardiol* **58**, 125–133.

Despa S, Islam MA, Pogwizd SM & Bers DM (2002). Intracellular $[Na^+]$ and Na^+ pump rate in rat and rabbit ventricular myocytes. *J Physiol* **539**, 133–143.

Domeier TL, Blatter LA & Zima AV (2009). Alteration of sarcoplasmic reticulum Ca^{2+} release termination by ryanodine receptor sensitization and in heart failure. *J Physiol* **587**, 5197–5209.

Domeier TL, Maxwell JT & Blatter LA (2012). β-Adrenergic stimulation increases the intra-sarcoplasmic reticulum Ca^{2+} threshold for Ca^{2+} wave generation. *J Physiol* **590**, 6093–6108.

Domeier TL, Zima AV, Maxwell JT, Huke S, Mignery GA & Blatter LA (2008). IP_3 receptor-dependent Ca^{2+} release modulates excitation–contraction coupling in rabbit ventricular myocytes. *Am J Physiol Heart Circ Physiol* **294**, H596–H604.

Dominic EA, Ramezani A, Anker SD, Verma M, Mehta N & Rao M (2014). Mitochondrial cytopathies and cardiovascular disease. *Heart* **100**, 611–618.

Drummond GB (2009). Reporting ethical matters in *The Journal of Physiology*: standards and advice. *J Physiol* **587**, 713–719.

Foskett JK, White C, Cheung KH & Mak DO (2007). Inositol trisphosphate receptor Ca^{2+} release channels. *Physiol Rev* **87**, 593–658.

Go LO, Moschella MC, Watras J, Handa KK, Fyfe BS & Marks AR (1995). Differential regulation of two types of intracellular calcium release channels during end-stage heart failure. *J Clin Invest* **95**, 888–894.

Harzheim D, Movassagh M, Foo RS, Ritter O, Tashfeen A, Conway SJ, Bootman MD & Roderick HL (2009). Increased $InsP_3Rs$ in the junctional sarcoplasmic reticulum augment Ca^{2+} transients and arrhythmias associated with cardiac hypertrophy. *Proc Natl Acad Sci USA* **106**, 11406–11411.

Hohendanner F, Ljubojevic S, Macquaide N, Sacherer M, Sedej S, Biesmans L, Wakula P, Platzer D, Sokolow S, Herchuelz A *et al.* (2013). Intracellular dyssynchrony of diastolic cytosolic $[Ca^{2+}]$ decay in ventricular cardiomyocytes in cardiac remodeling and human heart failure. *Circ Res* **113**, 527–538.

Huser J, Lipsius SL & Blatter LA (1996). Calcium gradients during excitation–contraction coupling in cat atrial myocytes. *J Physiol* **494**, 641–651.

Johnstone D, Limacher M, Rousseau M, Liang CS, Ekelund L, Herman M, Stewart D, Guillotte M, Bjerken G, Gaasch W *et al.* (1992). Clinical characteristics of patients in studies of left ventricular dysfunction (SOLVD). *Am J Cardiol* **70**, 894–900.

Kapoor N, Maxwell JT, Mignery GA, Will D, Blatter LA & Banach K (2014). Spatially defined $InsP_3$-mediated signaling in embryonic stem cell-derived cardiomyocytes. *PLoS One* **9**, e83715.

Kettlewell S, Burton FL, Smith GL & Workman AJ (2013). Chronic myocardial infarction promotes atrial action potential alternans, afterdepolarizations, and fibrillation. *Cardiovasc Res* **99**, 215–224.

Kettlewell S, Cabrero P, Nicklin SA, Dow JA, Davies S & Smith GL (2009). Changes of intra-mitochondrial Ca^{2+} in adult ventricular cardiomyocytes examined using a novel fluorescent Ca^{2+} indicator targeted to mitochondria. *J Mol Cell Cardiol* **46**, 891–901.

Kockskamper J, Sheehan KA, Bare DJ, Lipsius SL, Mignery GA & Blatter LA (2001). Activation and propagation of Ca^{2+} release during excitation–contraction coupling in atrial myocytes. *Biophys J* **81**, 2590–2605.

Kockskamper J, Zima AV, Roderick HL, Pieske B, Blatter LA & Bootman MD (2008). Emerging roles of inositol 1,4,5-trisphosphate signaling in cardiac myocytes. *J Mol Cell Cardiol* **45**, 128–147.

Li Q, O'Neill SC, Tao T, Li Y, Eisner D & Zhang H (2012). Mechanisms by which cytoplasmic calcium wave propagation and alternans are generated in cardiac atrial myocytes lacking T-tubules-insights from a simulation study. *Biophys J* **102**, 1471–1482.

Li X, Zima AV, Sheikh F, Blatter LA & Chen J (2005). Endothelin-1-induced arrhythmogenic Ca^{2+} signaling is abolished in atrial myocytes of inositol-1,4,5-trisphosphate (IP_3)-receptor type 2-deficient mice. *Circ Res* **96**, 1274–1281.

Linderer T, Chatterjee K, Parmley WW, Sievers RE, Glantz SA & Tyberg JV (1983). Influence of atrial systole on the Frank–Starling relation and the end-diastolic pressure–diameter relation of the left ventricle. *Circulation* **67**, 1045–1053.

Lipp P, Laine M, Tovey SC, Burrell KM, Berridge MJ, Li W & Bootman MD (2000). Functional $InsP_3$ receptors that may modulate excitation–contraction coupling in the heart. *Curr Biol* **10**, 939–942.

Mackenzie L, Roderick HL, Berridge MJ, Conway SJ & Bootman MD (2004). The spatial pattern of atrial cardiomyocyte calcium signalling modulates contraction. *J Cell Sci* **117**, 6327–6337.

Majerus PW, Kisseleva MV & Norris FA (1999). The role of phosphatases in inositol signaling reactions. *J Biol Chem* **274**, 10669–10672.

Matlib MA, Zhou Z, Knight S, Ahmed S, Choi KM, Krause-Bauer J, Phillips R, Altschuld R, Katsube Y, Sperelakis N & Bers DM (1998). Oxygen-bridged dinuclear ruthenium amine complex specifically inhibits Ca^{2+} uptake into mitochondria *in vitro* and *in situ* in single cardiac myocytes. *J Biol Chem* **273**, 10223–10231.

Maxwell JT & Blatter LA (2012). Facilitation of cytosolic calcium wave propagation by local calcium uptake into the sarcoplasmic reticulum in cardiac myocytes. *J Physiol* **590**, 6037–6045.

Maxwell JT, Domeier TL & Blatter LA (2012). Dantrolene prevents arrhythmogenic Ca release in heart failure. *Am J Physiol Heart Circ Physiol* **302**, H953–H963.

Meissner A, Min JY & Simon R (1998). Effects of angiotensin II on inotropy and intracellular Ca^{2+} handling in normal and hypertrophied rat myocardium. *J Mol Cell Cardiol* **30**, 2507–2518.

Miyata H, Silverman HS, Sollott SJ, Lakatta EG, Stern MD & Hansford RG (1991). Measurement of mitochondrial free Ca^{2+} concentration in living single rat cardiac myocytes. *Am J Physiol Heart Circ Physiol* **261**, H1123–H1134.

Nattel S (2002). New ideas about atrial fibrillation 50 years on. *Nature* **415**, 219–226.

Nicod P, Hillis LD, Winniford MD & Firth BG (1986). Importance of the "atrial kick" in determining the effective mitral valve orifice area in mitral stenosis. *Am J Cardiol* **57**, 403–407.

O'Rourke B & Blatter LA (2009). Mitochondrial Ca^{2+} uptake: tortoise or hare? *J Mol Cell Cardiol* **46**, 767–774.

Peppiatt CM, Collins TJ, Mackenzie L, Conway SJ, Holmes AB, Bootman MD, Berridge MJ, Seo JT & Roderick HL (2003). 2-Aminoethoxydiphenyl borate (2-APB) antagonises inositol 1,4,5-trisphosphate-induced calcium release, inhibits calcium pumps and has a use-dependent and slowly reversible action on store-operated calcium entry channels. *Cell Calcium* **34**, 97–108.

Picht E, Zima AV, Blatter LA & Bers DM (2007). SparkMaster: automated calcium spark analysis with ImageJ. *Am J Physiol Cell Physiol* **293**, C1073–C1081.

Pogwizd SM (1995). Nonreentrant mechanisms underlying spontaneous ventricular arrhythmias in a model of nonischemic heart failure in rabbits. *Circulation* **92**, 1034–1048.

Pogwizd SM, Qi M, Yuan W, Samarel AM & Bers DM (1999). Upregulation of Na^+/Ca^{2+} exchanger expression and function in an arrhythmogenic rabbit model of heart failure. *Circ Res* **85**, 1009–1019.

Pogwizd SM, Schlotthauer K, Li L, Yuan W & Bers DM (2001). Arrhythmogenesis and contractile dysfunction in heart failure: Roles of sodium–calcium exchange, inward rectifier potassium current, and residual β-adrenergic responsiveness. *Circ Res* **88**, 1159–1167.

Rahimtoola SH, Ehsani A, Sinno MZ, Loeb HS, Rosen KM & Gunnar RM (1975). Left atrial transport function in myocardial infarction. Importance of its booster pump function. *Am J Med* **59**, 686–694.

Raymond RJ, Lee AJ, Messineo FC, Manning WJ & Silverman DI (1998). Cardiac performance early after cardioversion from atrial fibrillation. *Am Heart J* **136**, 435–442.

Remus TP, Zima AV, Bossuyt J, Bare DJ, Martin JL, Blatter LA, Bers DM & Mignery GA (2006). Biosensors to measure inositol 1,4,5-trisphosphate concentration in living cells with spatiotemporal resolution. *J Biol Chem* **281**, 608–616.

Sedova M, Dedkova EN & Blatter LA (2006). Integration of rapid cytosolic Ca^{2+} signals by mitochondria in cat ventricular myocytes. *Am J Physiol Cell Physiol* **291**, C840–C850.

Shannon TR, Pogwizd SM & Bers DM (2003). Elevated sarcoplasmic reticulum Ca^{2+} leak in intact ventricular myocytes from rabbits in heart failure. *Circ Res* **93**, 592–594.

Sheehan KA & Blatter LA (2003). Regulation of junctional and non-junctional sarcoplasmic reticulum calcium release in

excitation–contraction coupling in cat atrial myocytes. *J Physiol* **546**, 119–135.
Sheehan KA, Zima AV & Blatter LA (2006). Regional differences in spontaneous Ca^{2+} spark activity and regulation in cat atrial myocytes. *J Physiol* **572**, 799–809.
Shkryl VM, Maxwell JT & Blatter LA (2011). A novel method for spatially complex diffraction-limited photoactivation and photobleaching in living cells. *J Physiol* **590**, 1093–1100.
Solaro RJ & Briggs FN (1974). Estimating the functional capabilities of sarcoplasmic reticulum in cardiac muscle. Calcium binding. *Circ Res* **34**, 531–540.
Stern MD, Song LS, Cheng H, Sham JS, Yang HT, Boheler KR & Rios E (1999). Local control models of cardiac excitation–contraction coupling. A possible role for allosteric interactions between ryanodine receptors. *J Gen Physiol* **113**, 469–489.
Thul R, Coombes S, Roderick HL & Bootman MD (2012). Subcellular calcium dynamics in a whole-cell model of an atrial myocyte. *Proc Natl Acad Sci USA* **109**, 2150–2155.
Tovey SC, de Smet P, Lipp P, Thomas D, Young KW, Missiaen L, De Smedt H, Parys JB, Berridge MJ, Thuring J, Holmes A & Bootman MD (2001). Calcium puffs are generic $InsP_3$-activated elementary calcium signals and are downregulated by prolonged hormonal stimulation to inhibit cellular calcium responses. *J Cell Sci* **114**, 3979–3989.
Trafford AW, Clarke JD, Richards MA, Eisner DA & Dibb KM (2013). Calcium signalling microdomains and the t-tubular system in atrial mycoytes: potential roles in cardiac disease and arrhythmias. *Cardiovasc Res* **98**, 192–203.
Tsang TS, Gersh BJ, Appleton CP, Tajik AJ, Barnes ME, Bailey KR, Oh JK, Leibson C, Montgomery SC & Seward JB (2002). Left ventricular diastolic dysfunction as a predictor of the first diagnosed nonvalvular atrial fibrillation in 840 elderly men and women. *J Am Coll Cardiol* **40**, 1636–1644.
Vasilevski O, Grubb DR, Filtz TM, Yang S, McLeod-Dryden TJ, Luo J, Karna D, Chen J & Woodcock EA (2008). $Ins(1,4,5)P_3$ regulates phospholipase Cβ1 expression in cardiomyocytes. *J Mol Cell Cardiol* **45**, 679–684.
Wang TJ, Larson MG, Levy D, Vasan RS, Leip EP, Wolf PA, D'Agostino RB, Murabito JM, Kannel WB & Benjamin EJ (2003). Temporal relations of atrial fibrillation and congestive heart failure and their joint influence on mortality: the Framingham Heart Study. *Circulation* **107**, 2920–2925.
Wendt-Gallitelli MF & Isenberg G (1989). X-ray microanalysis of single cardiac myocytes frozen under voltage-clamp conditions. *Am J Physiol Heart Circ Physiol* **256**, H574–H583.
Wijffels MC, Kirchhof CJ, Dorland R, Power J & Allessie MA (1997). Electrical remodeling due to atrial fibrillation in chronically instrumented conscious goats: roles of neurohumoral changes, ischemia, atrial stretch, and high rate of electrical activation. *Circulation* **96**, 3710–3720.
Yamda J, Ohkusa T, Nao T, Ueyama T, Yano M, Kobayashi S, Hamano K, Esato K & Matsuzaki M (2001). Up-regulation of inositol 1,4,5 trisphosphate receptor expression in atrial tissue in patients with chronic atrial fibrillation. *J Am Coll Cardiol* **37**, 1111–1119.
Zhao ZH, Zhang HC, Xu Y, Zhang P, Li XB, Liu YS & Guo JH (2007). Inositol-1,4,5-trisphosphate and ryanodine-dependent Ca^{2+} signaling in a chronic dog model of atrial fibrillation. *Cardiology* **107**, 269–276.
Zima AV & Blatter LA (2004). Inositol-1,4,5-trisphosphate-dependent Ca^{2+} signalling in cat atrial excitation–contraction coupling and arrhythmias. *J Physiol* **555**, 607–615.
Zima AV, Bovo E, Bers DM & Blatter LA (2010). Ca^{2+} spark-dependent and -independent sarcoplasmic reticulum Ca^{2+} leak in normal and failing rabbit ventricular myocytes. *J Physiol* **588**, 4743–4757.
Zima AV, Pabbidi MR, Lipsius SL & Blatter LA (2013). Effects of mitochondrial uncoupling on Ca^{2+} signaling during excitation–contraction coupling in atrial myocytes. *Am J Physiol Heart Circ Physiol* **304**, H983–H993.

Additional information

Competing interests

None declared.

Author contributions

Conception and design of the experiments: F.H, L.A.B. Collection, analysis and interpretation of data: F.H., S.W., J.T.M. S.K., S.A., G.L.S., V.A.L., L.A.B. Drafting the article: F.H., L.A.B. All authors have approved the final version of the manuscript.

Funding

This work was supported by National Institutes of Health grants HL62231, HL80101 and HL101235 and the Leducq Foundation (to L.A.B.).